G-PFEM: a Particle Finite Element Method platform for geotechnical applications.

L. Monforte, M. Arroyo, J.M. Carbonell[1] & A. Gens
Universitat Politècnica de Catalunya, BarcelonaTech
[1]CIMNE, International Center for Numerical Methods in Engineering

Outline

- Motivation
- Numerical model
  - Particle Finite Element Method
  - Constitutive equations
  - Contact constraints
- Mixed formulations
  - Mixed formulations for the one-phase problem
  - Mixed formulations for the hydro-mechanical problem
- Application analyses
  - Soil sampler
- Conclusions

Motivation: in situ test

Cone penetration test is one of the most widely used in situ test.

The interpretation of the test -the relation between reaction and soil constitutive parameters- is still based on empiricism.

Numerical analysis of penetration problems may increase the confidence of interpretation of in-situ tests.

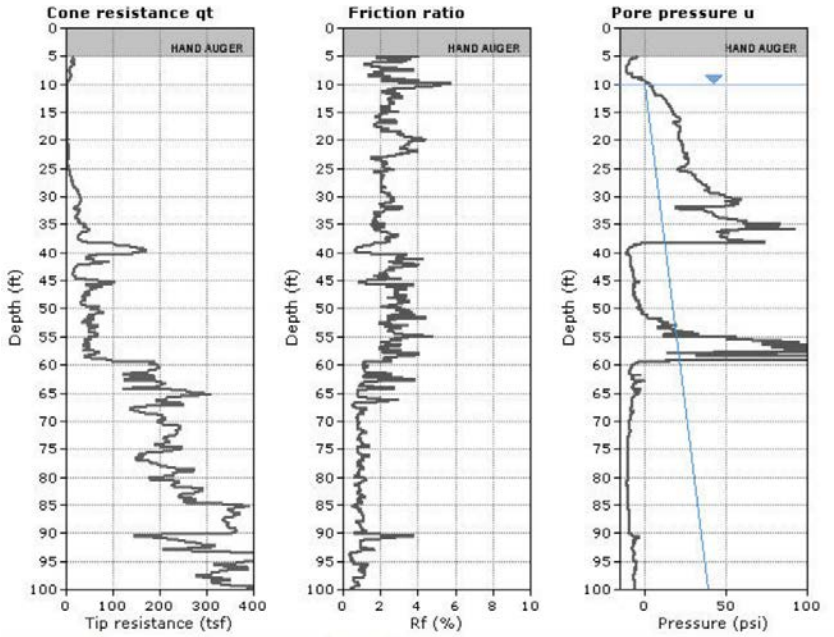

Piles

Boylan et al (2017)

Samplers & Corers

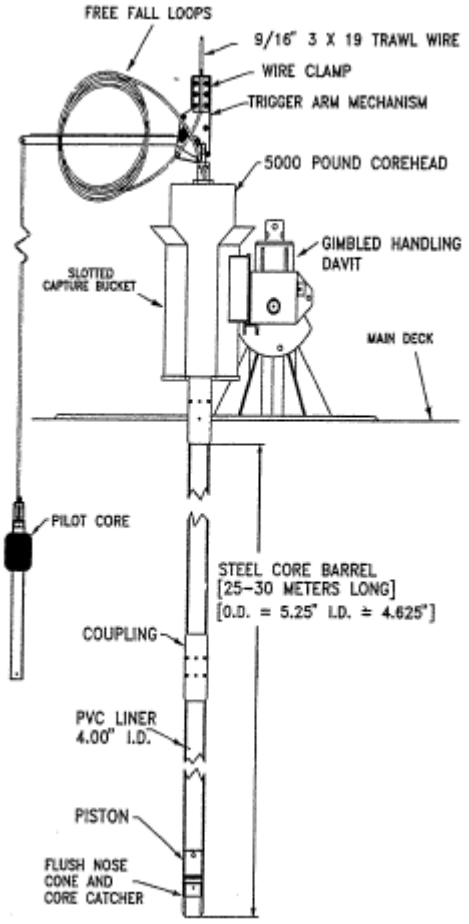

Silva & Bryant (1989)

Sampling disturbance

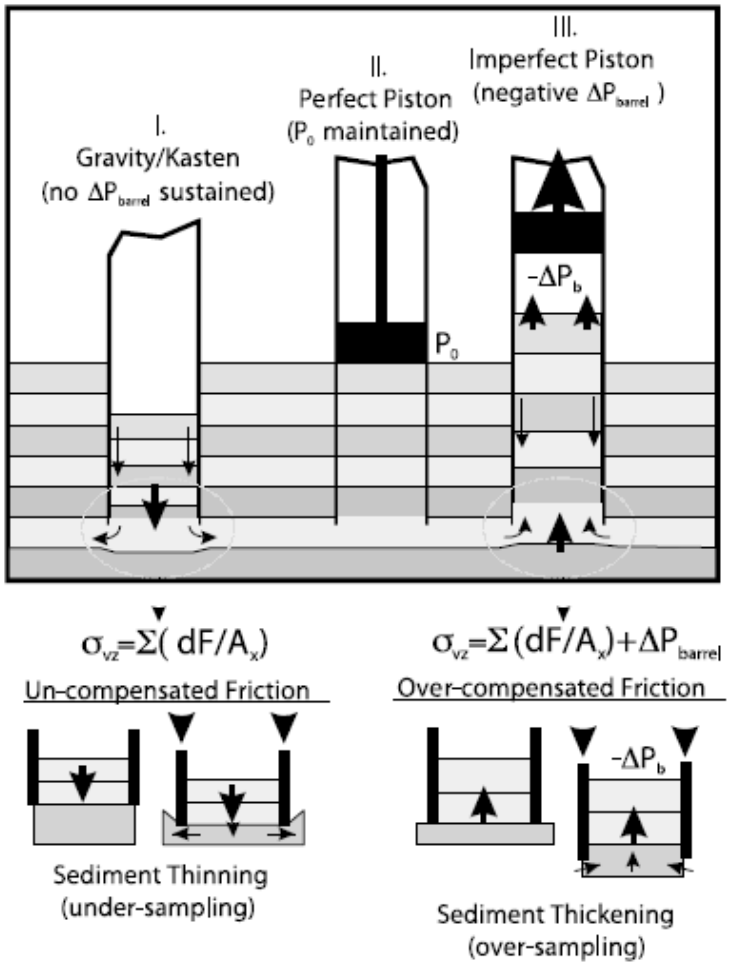

Skinner & McCabe (2003)

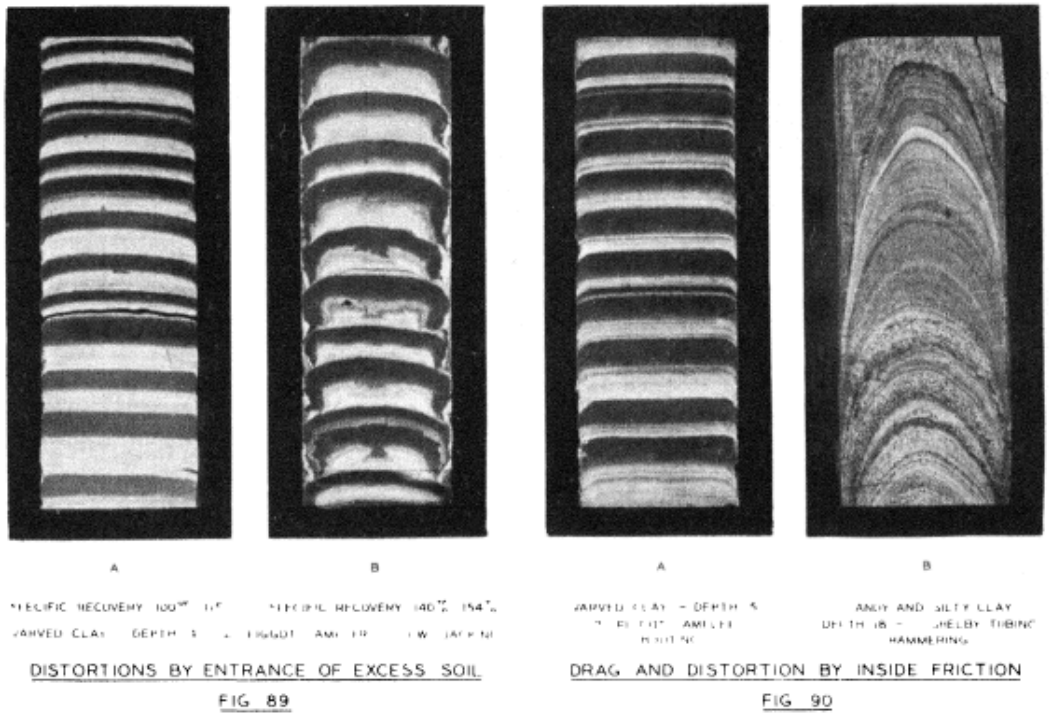

Hvorslev (1949)

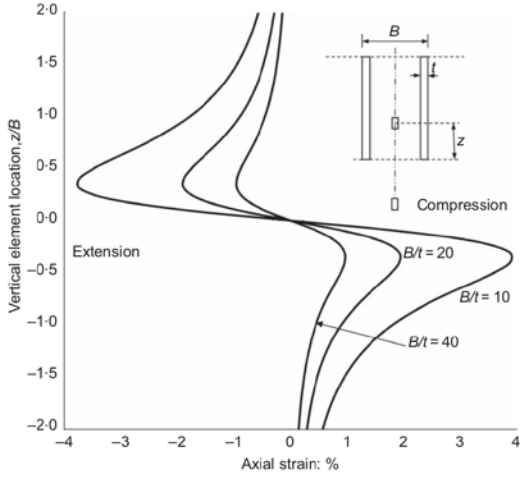

Baligh et al (1987)

Motivation: sampling

Sampling can cause significant disturbance so that the samples obtained do not truly reflect the in situ state.

Soil sampler geometry and roughness plays a prominent role in the disturbance of the soil.

It is believed that the vertical strain along the symmetry axis is a good estimator of the sample disturbance (Baligh et al, 1987).

The Strain Path Method (Baligh et al, 1987) has been extensively used to simulate the tube sampling process.

Very few numerical simulations have been performed (Alonso & Oñate, 1981; Budhu & Wu, 1992).

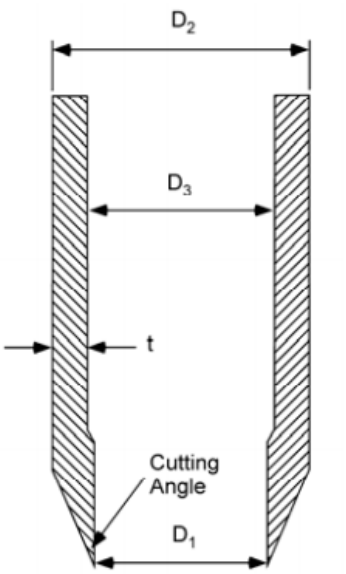

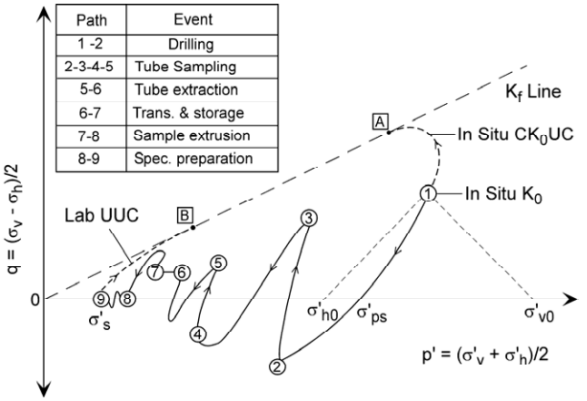

(de Groot et al, 2005)

(Hover et al, 2013)

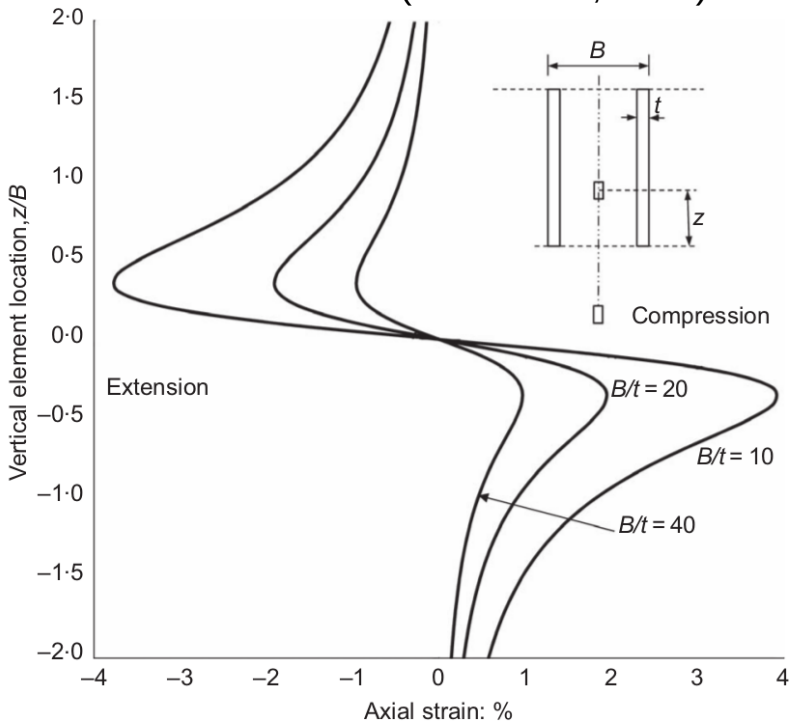

Motivation

- The simulation is a complex task since it is a system full of nonlinearities:
  - Material
  - Geometrical
  - Contact (normal and tangent)
- Additionally, the occurrence of an incompressible response of the medium may pose additional numerical difficulties.

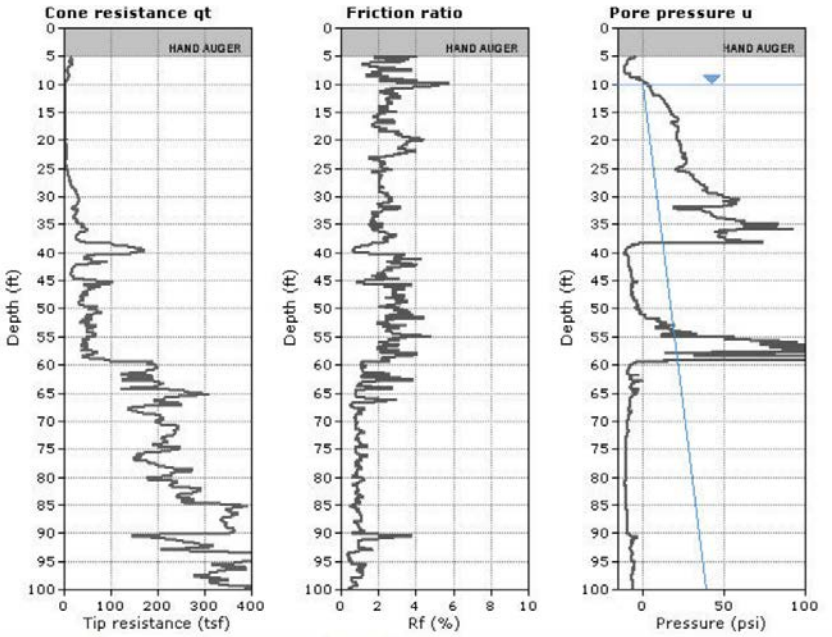

Outline

- Motivation
- ***Numerical model***
  - ***Particle Finite Element Method***
  - ***Constitutive equations***
  - ***Contact constraints***
- Mixed formulations
  - Mixed formulations for the one-phase problem
  - Mixed formulations for the hydro-mechanical problem
- Application analyses
  - Soil sampler
- Conclusions

Particle finite element method (Oñate et al, 2004, 2008)

- The nodes of the domain as treated as particles whose motion is tracked during the solution process
- The particles serves as nodes of a Finite Elemet mesh
  - The FE mesh is periodically re-triangulated
  - h-apdative methods are used:
    - Insertion of nodes in regions with large plastic dissipation
    - Remove of nodes due to local concentration of particles and in the elastic part of the domain.
- The continuum is modelled using an Updated Lagrangrian formulation.
- Only low order elements are used. (Prone to volumetric locking)

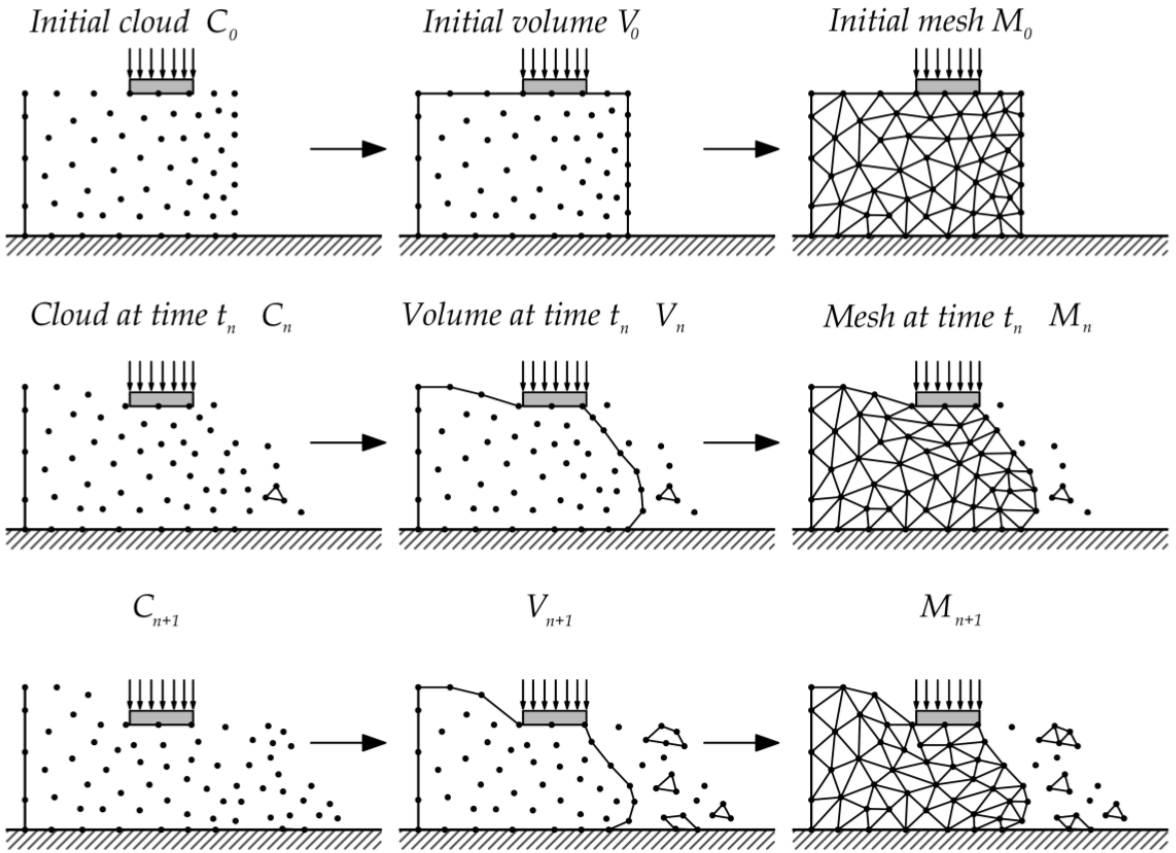

Balance equations

For the single-phase medium, the linear momentum balance equation may be written as:

$$\begin{cases} \nabla \cdot \boldsymbol{\sigma} + \mathbf{b} = \mathbf{0} & \text{in } \Omega_t \times (0,T) \\ \boldsymbol{u}(\boldsymbol{X}, t=0) = \boldsymbol{u}_0 & \text{in } \Omega_0 \\ \boldsymbol{u}(\boldsymbol{X}, t) = \bar{\boldsymbol{u}} & \text{in } \Gamma_u \times (0,T) \\ \boldsymbol{n} \cdot \boldsymbol{\sigma} = \bar{\boldsymbol{t}} & \text{in } \Gamma_{\bar{t}} \times (0,T) \end{cases}$$

where $\boldsymbol{\sigma} = \hat{\boldsymbol{\sigma}}(\boldsymbol{F}, V)$ is the Cauchy stress tensor.

The balance of mass and linear momentum for a fluid-saturated porous media read using an Updated Lagrangian form (with respect to the solid-phase) reads (Larsson & Larsson, 2002):

$$\begin{cases} \nabla \cdot \boldsymbol{\sigma} + \mathbf{b} = 0 & \text{in } \Omega_t \times (0,T) \\ \dfrac{-1}{\kappa_w} \dot{p}_w + \nabla \cdot \mathbf{v} + \nabla \cdot \mathbf{v}^d = 0 & \text{in } \Omega_t \times (0,T) \end{cases}$$

where, according to the effective stress principle: $\boldsymbol{\sigma} = \boldsymbol{\sigma}' + p_w \mathbb{1} = \hat{\boldsymbol{\sigma}}'(\boldsymbol{F}, V) + p_w \mathbb{1}$

The principal assumptions are:

- Fluid-saturated porous media,
- Quasi-static,
- The solid phase is composed by incompressible particles whereas the liquid is almost incompressible.

Numerical treatment

- Low order shape functions are used.
- Use of an Updated Lagrangian formulation.
- An implicit time integration algorithm,
- In the hidro-mechanical problem, (Solid skeleton) displacement and water pressure are the unknown fields (***u***-p_w formulation),

$$\mathbf{P}\left({}^{n+1}\boldsymbol{\sigma}\right) = {}^{n+1}\,\mathbf{f}^{ext}$$

$$\begin{cases} \mathbf{P}\left({}^{n+1}\boldsymbol{\sigma}'\right) + \mathbf{Q}\cdot{}^{n+1}\,\tilde{\mathbf{p}}_w = \mathbf{f}^{ext} \\ \mathbf{Q}^{\star T}\cdot\Delta\tilde{\mathbf{u}} - \dfrac{1}{K_w}\mathbf{M}\cdot\Delta\tilde{\mathbf{p}}_w - \Delta t\,\mathbf{H}\cdot{}^{n+1}\,\tilde{\mathbf{p}}_w = \Delta t\,\mathbf{f}^{p_w} \end{cases}$$

$$\mathbf{P}(\boldsymbol{\sigma}) = \int_{\Omega_t}\mathbf{B}^T\cdot\underline{\boldsymbol{\sigma}}\;\mathrm{d}\Omega_t$$

$$\mathbf{Q} = \int_{\Omega_t}\mathbf{B}^T\cdot\underline{\mathbb{1}}\cdot\mathbf{N}\;\mathrm{d}\Omega_t$$

$$\mathbf{Q}^{\star T} = \int_{\Omega_t}\mathbf{N}^T\cdot\underline{\mathbb{1}}\cdot\mathbf{B}\frac{1}{J}\;\mathrm{d}\Omega_t$$

$$\mathbf{f}^{ext} = \int_{\Omega_t}\mathbf{N}_u^T\cdot\mathbf{b}\;\mathrm{d}\Omega_t + \int_{\Gamma_{\bar{t}}}\mathbf{N}_u^T\cdot\bar{\mathbf{t}}\;\mathrm{d}\gamma_t$$

$$\mathbf{M} = \int_{\Omega_t}\mathbf{N}^T\cdot\mathbf{N}\frac{1}{J}\;\mathrm{d}\Omega_t$$

$$\mathbf{H} = \int_{\Omega_t}(\nabla\mathbf{N})^T\cdot\mathbf{k}_p\cdot(\nabla\mathbf{N})\frac{1}{J}\;\mathrm{d}\Omega_t$$

$$\mathbf{f}^{p_w} = \int_{\Omega t}(\nabla\mathbf{N})^T\cdot\boldsymbol{k}\cdot\mathbf{g}\;\frac{\rho_w}{J}\;\mathrm{d}\Omega_t + \int_{\Gamma_g}(\nabla\mathbf{N})^T\overline{g}\frac{1}{J}\;\mathrm{d}\Gamma$$

Constitutive frameworks

	Hyper-elastic based plasticity $\boldsymbol{F = F^e \cdot F^p}$	Hypo-elastic based plasticity $\boldsymbol{d = d^e + d^p}$	
Explicit integration	***This work***	Bathe (1996) Nazem et al (2006, 2009)	Often found more robust. More laborious algorithms.
Implicit integration	Simo (1998) Simo & Hughes (1998) Rouainia & Muir Wood (2000) Pérez-Foguet & Armero (2002)	Simo & Hughes (1998)	Second order convergence of the global problem. Lack of convergence for complex plastic models.
	Mutliplicative split of the deformation gradient. The formulation is inherently frame indifferent.	Additive split of the spatial rate of deformation. Use of an objective stress rate.	

Constitutive equations

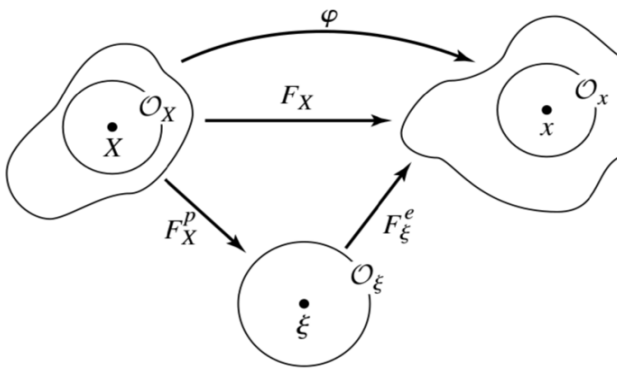

The local problem is given by (Simo, 1998):

$$\begin{cases} \text{Strain decomposition:} & \boldsymbol{F} = \frac{\partial \boldsymbol{x}}{\partial \boldsymbol{X}} = \boldsymbol{F}^e \cdot \boldsymbol{F}^p \\ \text{Hyperelastic model:} & \boldsymbol{\tau} = J\boldsymbol{\sigma} = W(\boldsymbol{F}^e \cdot \boldsymbol{F}^{eT}) \\ \text{Yield surface:} & f(\boldsymbol{\tau}, V) \leq 0 \\ \text{Flow rule:} & \boldsymbol{l}^p = \dot{\lambda} \frac{\partial G(\boldsymbol{\tau}, V)}{\partial \boldsymbol{\tau}} \quad \text{where} \quad \boldsymbol{l}^p = \boldsymbol{F}^e \cdot \overline{\boldsymbol{L}}^p \cdot (\boldsymbol{F}^e)^{-1} \\ \text{Hardening law:} & V = V(\boldsymbol{F}^p \cdot \boldsymbol{F}^{pT}) \end{cases}$$

Assuming an exponential variation of the deformation gradient, the following explicit expression is obtained for the Elastic Left Cauchy Green tensor:

$$\mathbf{b}^e_{n+1} = \mathbf{F}_{n+1} \cdot \mathbf{F}_n^{-1} \cdot \exp\left(-\Delta\gamma \left.\frac{\partial G(\boldsymbol{\tau}, h)}{\partial \boldsymbol{\tau}}\right|_n\right) \cdot \mathbf{b}^e_n \cdot \exp\left(-\Delta\gamma \left.\frac{\partial G(\boldsymbol{\tau}, h)}{\partial \boldsymbol{\tau}}\right|_n\right)^T \cdot \mathbf{F}_n^{-T} \cdot \mathbf{F}_{n+1}^T$$

where the Plastic multiplier may be approximated as:

$$\Delta\gamma = \frac{\frac{\partial f}{\partial \boldsymbol{\tau}} : \mathbb{D}^e : \nabla\Delta\mathbf{u}}{H + \frac{\partial f}{\partial \boldsymbol{\tau}} : \mathbb{D}^e : \frac{\partial G(\boldsymbol{\tau}, h)}{\partial \boldsymbol{\tau}}}$$

whereas the Elasto-Plastic matrix:

$$\mathcal{L}_v\boldsymbol{\tau} = \mathbb{D}^e : \mathbf{d}^e = \left(\mathbb{D}^e - \frac{\mathbb{D}^e : \partial_{\boldsymbol{\tau}} G \otimes \partial_{\boldsymbol{\tau}} \psi : \mathbb{D}^e}{H + \partial_{\boldsymbol{\tau}} \psi : \mathbb{D}^e : \partial_{\boldsymbol{\tau}} G}\right) : \mathbf{d}$$

The general algorithm to integrate elasto-plastic relations is based on Sloan et al (2001).

Additionally, to reduce the computational cost and increase the computability an IMPLEX algorithm (Oliver, 2008) is used.

Sloan et al (2001) algorithm

To overcome the shortcomings of explicit integration algorithms, Sloan et al (2001) algorithm is used:

- (First order in time): Adaptive substepping.
- (Violation of the yield surface): Drift correction algorithm.

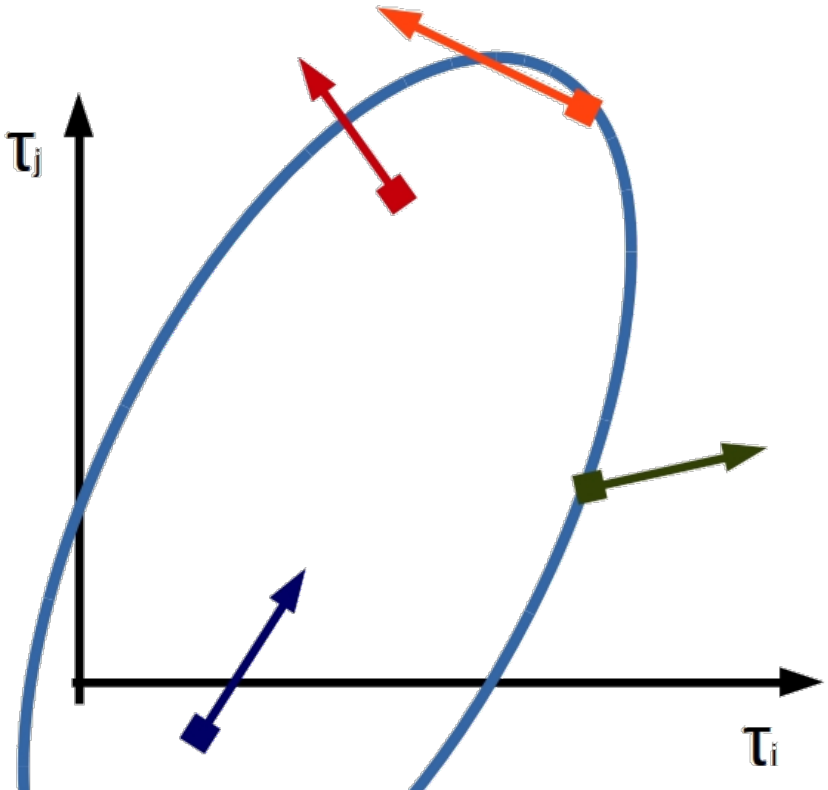

Algorithm 1: Stress integration with error control

Data: b_n^e, h_n, f_n^{n+1}

$\Psi^0 = \Psi(\tau_n, h_n)$

$\tau_{n+1}^{tr} = W(f_n^{n+1} \cdot b_n^e \cdot f_n^{n+1T})$

$\Psi^{tr} = \Psi(\tau_{n+1}^{tr}, h_n)$

if $\Psi^{tr} < TOL$ **then**

  $b_{n+1}^e = f_n^{n+1} \cdot b_n^e \cdot f_n^{n+1T}$

  $h_{n+1} = h_n$;

else

  $\text{Flag}_1 = (\Psi^0 < -\text{Tol}_f \text{ and } \Psi^{tr} > \text{Tol}_f)$

  $\text{Flag}_2 = \left(\frac{\partial_\tau \Psi \cdot D_e \cdot \delta\epsilon}{\|\partial_\tau \Psi\| \|D_e \cdot \delta\epsilon\|} < \text{Tol}_L\right)$

  if *(Flag*$_1$ *or Flag*$_2$*)* **then**

    Find α such that $\Psi(W(b_{n+\alpha}^e), h_n) = 0$

    where $b_{n+\alpha}^e = f_n^{n+\alpha} b_n^e f_n^{n+\alpha T}$

    Set $h_{n+\alpha} = h_n$

  else

    $\alpha = 0$

  end

  while $\alpha < 1$ **do**

    Integrate elasto-plastic equations with substepping and error cont

  end

  Perform Drift Correction

end

$\tau_{n+1} = W(b_{n+1}^e)$

Result: $b_{n+1}^e, h_{n+1}, \tau_{n+1}$

Implex (Oliver et al, 2008)

The extremely non-linear behaviour of complex Elasto-Plastic materials may lead to a lack of convergence of the Global Problem.

Oliver et al (2008), developed the Implicit-Extrapolated scheme. Then the problem reads:

1. Solve the mechanical problem by using an extrapolated value of the plastic multiplier:

$$\begin{cases} \nabla \cdot \overline{\boldsymbol{\sigma}}_{n+1} + \mathbf{b} = \mathbf{0} & \\ \text{where:} & \overline{\boldsymbol{\sigma}}_{n+1} = \hat{\boldsymbol{\sigma}}(\mathbf{F}_{n+1}, V, \overline{\Delta\gamma}_n) \\ & \mathbf{b}^e_{n+1} = \mathbf{F}_{n+1} \cdot \mathbf{F}_n^{-1} \cdot \exp\left(\overline{\Delta\gamma}_n \, \partial_{\boldsymbol{\tau}} G_n\right) \cdot \mathbf{b}^e_n \cdot \exp\left(\overline{\Delta\gamma}_n \, \partial_{\boldsymbol{\tau}} G_n\right) \cdot \mathbf{F}_n^{-T} \cdot \mathbf{F}^T_{n+1} \\ & \mathcal{L}_v \boldsymbol{\tau} = \mathbb{D}^e : \mathbf{d} \end{cases}$$

2. Evaluation, at each Gauss point, of the constitutive model with the standard integration method.

$$\overline{\Delta\gamma}_{n+1} = \Delta\gamma_{n+1}$$

In some cases (small strains, linear elasticity, von Mises yield criterion) the problem becomes step-constant.

In a general problem, the number of required iterations to converge the Global problem is considerably reduced (Oliver et al, 2008).

Hyperelastic Modified Cam Clay

$$
\begin{cases}
\text{Hyperelasticity:} & \boldsymbol{\tau'} = \pi' \mathbb{1} + \boldsymbol{\tau}_d \\
\text{(Houlsby, 1985)} & \pi' = -p_0 \exp\left(\frac{-\epsilon_v^e}{\kappa^*}\right)\left(1 + \frac{\alpha}{\kappa^*}\|\epsilon_d^e\|^2\right) \\
\text{(Borja et al, 97)} & \boldsymbol{\tau}_d = 2\left(G_0 + \alpha\kappa^* \exp\left(\frac{-\epsilon_v^e}{\kappa^*}\right)\right)\epsilon_d^e \\
\text{Yield surface:} & f(\boldsymbol{\tau'}) = \left(\frac{\sqrt{3}J_2}{M(\theta_L)}\right)^2 + \pi'(\pi' - p_c) \\
\text{Flow rule:} & G = f \\
\text{Hardening law:} & p_c = p_{c0} \exp\left(\frac{-\epsilon_v^p}{\lambda^* - \kappa^*}\right)
\end{cases}
$$

where $\boldsymbol{\epsilon}^e = \frac{1}{2}\ln\left(\mathbf{F}^e \cdot \mathbf{F}^{e^T}\right)$; $\epsilon_v^e = \ln(J^e)$ and $\boldsymbol{\epsilon}_d^e = \frac{1}{2}\ln(\bar{\boldsymbol{b}}^e)$

Tresca model

$$
\begin{cases}
\text{Hyperelasticity:} & \boldsymbol{\tau} = K\,\epsilon_v^e\,\mathbb{1} + 2\,G\,\boldsymbol{\epsilon}_d^e \\
\text{Yield surface:} & f(\boldsymbol{\tau}) = J_2\,\cos(\theta_L) - S_u \\
\text{Flow rule:} & G = f
\end{cases}
$$

Contact

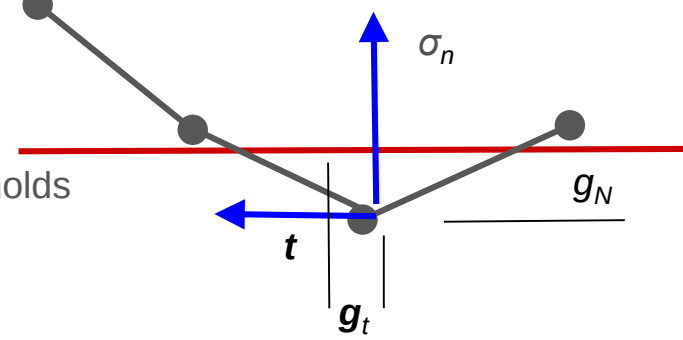

To simplify the problem, the structure is considered rigid; this hypothesis holds when the Young's moduli ratio between the structure and the soil is large (Wriggers, 2002). This way, the shape and movement of the structure is defined beforehand.

Contact constraints are introduced into the solution with the Penalty method (Wriggers, 2002):

$$\sum_{\gamma} \left(\int_{\Omega^{\gamma}_{n+1}} \nabla \mathbf{w} : \boldsymbol{\sigma} \, \mathrm{d}\Omega_{n+1} + \int_{\Omega^{\gamma}_{n+1}} \mathbf{w} \cdot \mathbf{b} \, \mathrm{d}\Omega_{n+1} + \int_{\Gamma^{\gamma}_{\sigma}} \mathbf{w} \cdot \mathbf{t}_{\sigma} \, \mathrm{d}\Gamma \right) + C_c = 0$$

$$C_c = \int_{\Gamma_c} \left(\mathbf{w}^2 - \overline{\mathbf{w}}^1 \right) \cdot \left(\sigma_n \overline{\mathbf{n}} + \mathbf{t} \right) d\Gamma$$

The normal part reads:

$$\sigma_n = \epsilon_N \; \overline{g_N}$$

In the tangential part, an elasto-plastic analogy is used (Wriggers, 2002). The yield surface depends on the normal effective stress:

$$\begin{cases} \mathbf{g}_T = \mathbf{g}^e + \mathbf{g}^s \\ \mathcal{L}_v \mathbf{t} = \epsilon_t \, \dot{\mathbf{g}}^e \\ f_s(\mathbf{t}, \sigma'_n, g_v) = \|\mathbf{t}\| - \overline{f}_s(\sigma'_n, g_v) \leq 0 \\ \dot{\mathbf{g}}^s = \dot{\gamma} \, \frac{\partial f_s}{\partial \boldsymbol{t}} = \dot{\gamma} \, \frac{\mathbf{t}}{\|\mathbf{t}\|} \\ \dot{g}_v = \dot{\gamma} \end{cases}$$

Outline

- Outline
- Numerical model
  - Particle Finite Element Method
  - Constitutive equations
  - Contact constraints
- ***Mixed formulations***
  - ***Mixed formulations for the one-phase problem***
  - ***Mixed formulations for the hydro-mechanical problem***
- Application analyses
  - Soil sampler
- Conclusions

Volumetric locking

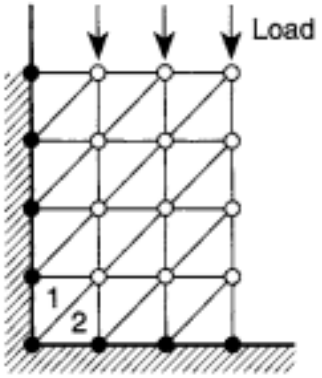

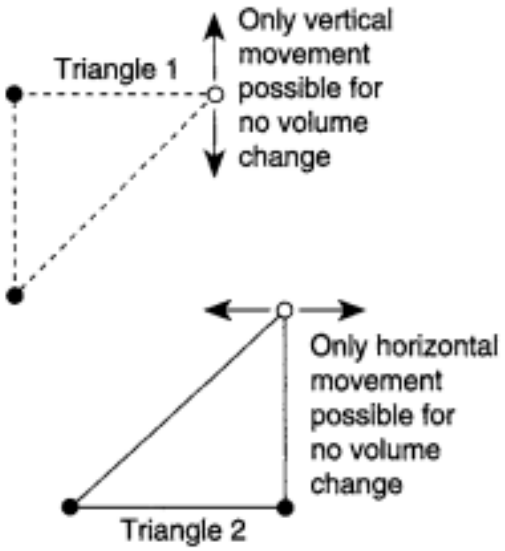

(Zienkiewicz et al, 2006)

Using FEM to describe incompressible materials may cause numerical problems or lead to an erroneous solution due to volumetric locking.

- This pathology is produced due to an overconstrained solution.
- Volumetric locking cause large oscillations at the pressure field and overestimates the reactions.
- Locking is more pronounced in low order elements.

Steel plate with a whole in at the center.
J2 plasticity with softening.

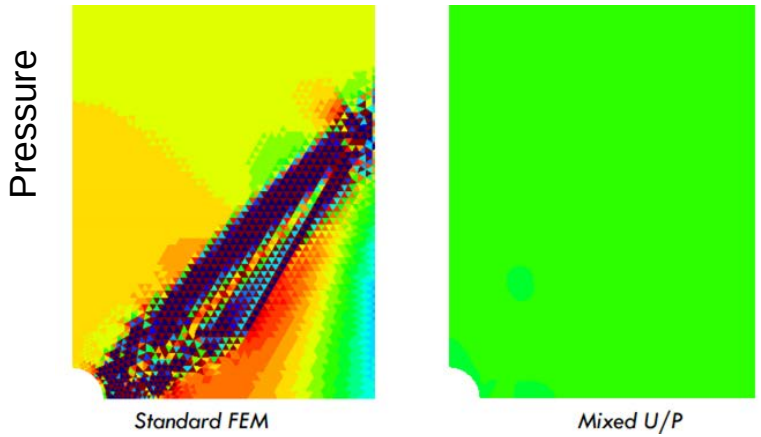

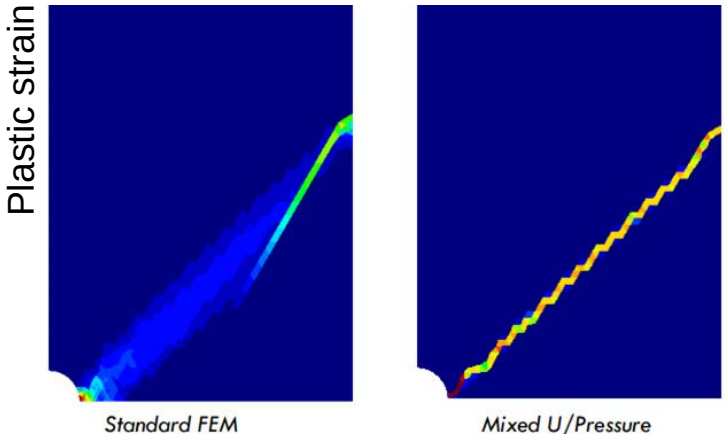

(Benedetti et al, 2015)

Volumetric locking

In total stress analysis, volumetric locking arises from the elasto-plastic constitutive models (i.e., incompressible elastic model and isochoric flow rule).

There are two sources of volumetric locking at the coupled hydro-mechanical problem:

- Compressible constitutive equations are used for the solid skeleton.
  - However, Critical state theory also predicts zero volume change at critical state (Sun et al, 2013).
- The mixture behaves like an incompressible material in almost undrained conditions (i.e. rapid application of loads with respect to the permeability).

Volumetric locking may be alleviated:

- Use of mixed stabilized formulations.
- For high-order elements:
  - Use of admissible elements in mixed formulations.
  - Use of smoothed volumetric strains.
  - Selective integration.

Mixed forms for the single phase problem

The three mixed formulations in strong form read:

$\mathbf{u} - p$:

$$\begin{cases} \nabla \cdot (\mathrm{dev}(\boldsymbol{\sigma}) + p\mathbb{1}) + \mathbf{b} = \mathbf{0} \\ p - (\frac{1}{3}\mathbb{1} : \boldsymbol{\sigma}) = 0 \end{cases}$$

$\mathbf{u} - \theta - p$, (Simo et al, 1985; Zienkiewicz et al 2006):

$$\begin{cases} \nabla \cdot \left(\left(\mathrm{dev}(\breve{\boldsymbol{\sigma}}) + \dfrac{J}{\theta} p\mathbb{1} \right) \dfrac{\theta}{J} \right) + \mathbf{b} = \mathbf{0} \\ J - \theta = 0 \\ p - (\dfrac{1}{3}\mathbb{1} : \breve{\boldsymbol{\sigma}}) = 0 \end{cases}$$

$$J = \det(\mathbf{F})$$

$$\breve{\boldsymbol{\sigma}} = \hat{\boldsymbol{\sigma}}(\breve{\boldsymbol{F}}.V)$$

$\mathbf{u} - \theta$:

$$\begin{cases} \nabla \cdot \breve{\boldsymbol{\sigma}} + \mathbf{b} = \mathbf{0} \\ J - \theta = 0 \end{cases}$$

$$\breve{\mathbf{F}} = \mathbf{F}^v \mathbf{F}^d = (\theta^{\frac{1}{3}})(\det(\mathbf{F})^{-\frac{1}{3}}\mathbf{F}) = \left(\frac{\theta}{\det(\mathbf{F})} \right)^{\frac{1}{3}} \mathbf{F}$$

Mixed forms for the single phase problem

In order to alleviate volumetric locking, the Polynomial Pressure Projection (Bochev et al, 2008) is applied to all scalar balance equations:

$$\int_{\Omega_0^e} (q - \breve{q}) \frac{\alpha_s}{\mu} (p - \breve{p})\, d\Omega_0 = 0$$

By using the PPP, a term proportional to the L2 norm of the difference of the approximation of the solution in C0 and the projection of the solution to a lower order shape functions is added to the residual.

Finally, the discrete FE equations read:

u-p
$$\begin{cases} \mathbf{P}(\mathrm{dev}(\boldsymbol{\sigma})) + \mathbf{Q} \cdot \tilde{\mathbf{p}} = \mathbf{f}^{ext} \\ (\mathbf{M} + \frac{\alpha_s^p}{\mu} \mathbf{M}^s) \cdot \tilde{\mathbf{p}} = \mathbf{f}^p(\boldsymbol{\sigma}) \end{cases}$$

u-J-p
$$\begin{cases} \mathbf{P}(\mathrm{dev}(\breve{\boldsymbol{\sigma}}) \frac{\theta}{J}) + \mathbf{Q} \cdot \tilde{\mathbf{p}} = \mathbf{f}^{ext} \\ (\mathbf{M} + \frac{\alpha_s^\theta}{\mu} \mathbf{M}^s) \cdot \tilde{\boldsymbol{\theta}} = \mathbf{f}^\theta \\ (\mathbf{M} + \frac{\alpha_s^p}{\mu} \mathbf{M}^s) \cdot \tilde{\mathbf{p}} = \mathbf{f}^p(\breve{\boldsymbol{\sigma}}) \end{cases}$$

u-J
$$\begin{cases} \mathbf{P}(\breve{\boldsymbol{\sigma}}) = \mathbf{f}^{ext} \\ (\mathbf{M} + \frac{\alpha_s^\theta}{\mu} \mathbf{M}^s) \cdot \tilde{\boldsymbol{\theta}} = \mathbf{f}^\theta \end{cases}$$

$$\mathbf{P}(\boldsymbol{\sigma}) = \int_{\Omega_t} \mathbf{B}^T \cdot \underline{\boldsymbol{\sigma}}\, d\Omega_t$$

$$\mathbf{Q} = \int_{\Omega_t} \mathbf{B}^T \cdot \underline{\mathbb{1}} \cdot \mathbf{N}\, d\Omega_t$$

$$\mathbf{M} = \int_{\Omega_t} \mathbf{N}^T \cdot \mathbf{N} \frac{1}{J}\, d\Omega_t$$

$$\mathbf{f}^{ext} = \int_{\Omega_t} \mathbf{N}_u^T \cdot \mathbf{b}\, d\Omega_t + \int_{\Gamma_{\bar{t}}} \mathbf{N}_u^T \cdot \bar{\mathbf{t}}\, d\Gamma$$

$$\mathbf{f}^\theta = \int_{\Omega_t} \mathbf{N}^T\, d\Omega_t$$

$$\mathbf{f}^p(\boldsymbol{\sigma}) = \int_{\Omega_t} \mathbf{N}^T (\frac{1}{3}\mathbb{1} : \boldsymbol{\sigma}) \frac{1}{J}\, d\Omega_t$$

$$\mathbf{M}^s = \int_{\Omega_t} \mathbf{N}^T \cdot \mathbf{N} \frac{1}{J}\, d\Omega_t - \int_{\Omega_t} \breve{\mathbf{N}}^T \cdot \breve{\mathbf{N}} \frac{1}{J}\, d\Omega_t$$

Strip footing on clay

Weightless uniform Tresca soil:

E = 100 kPa, S_u = 1 kPa, v = 0.495; $I_r = G/S_u$ = 33

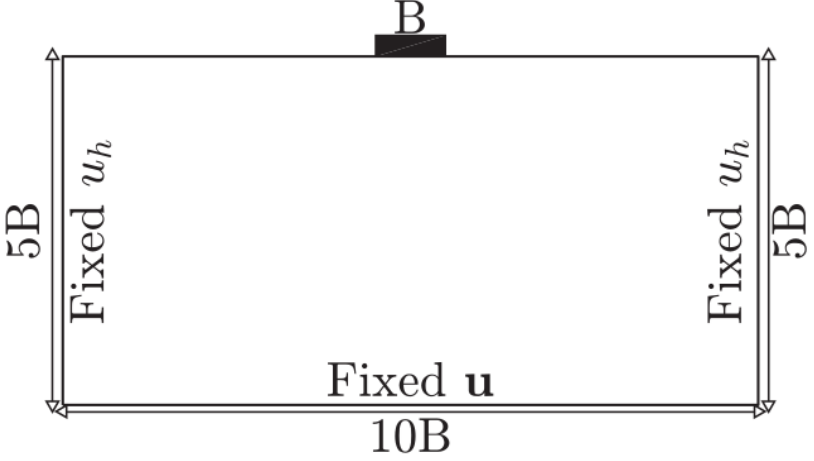

Total Vertical stress

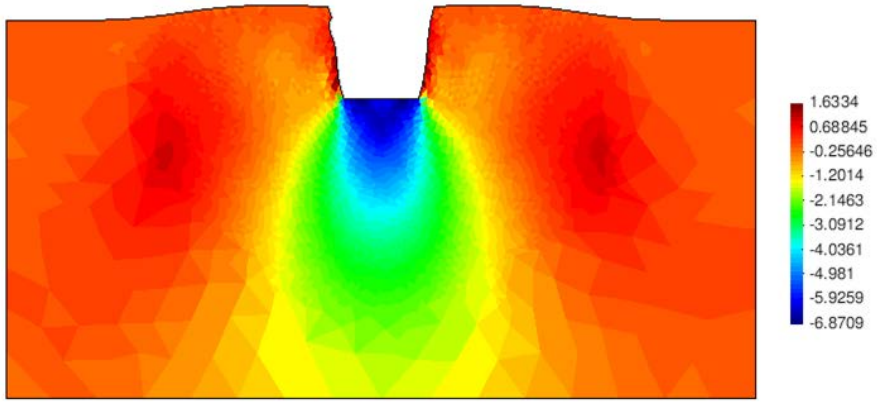

Incremental plastic shear strain

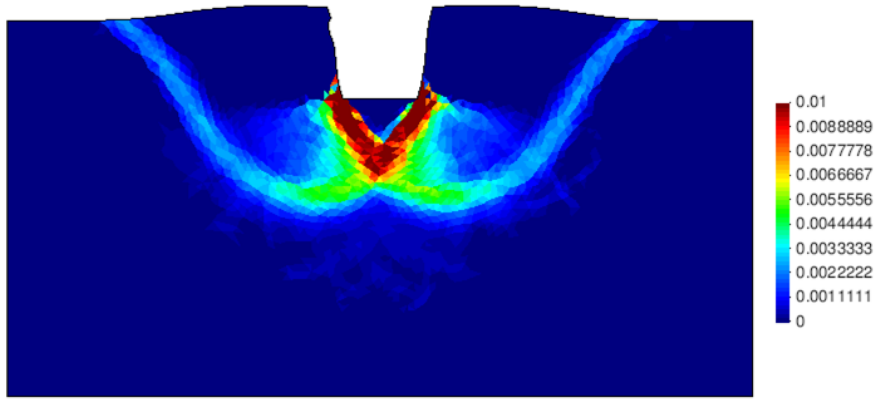

Total mean stress

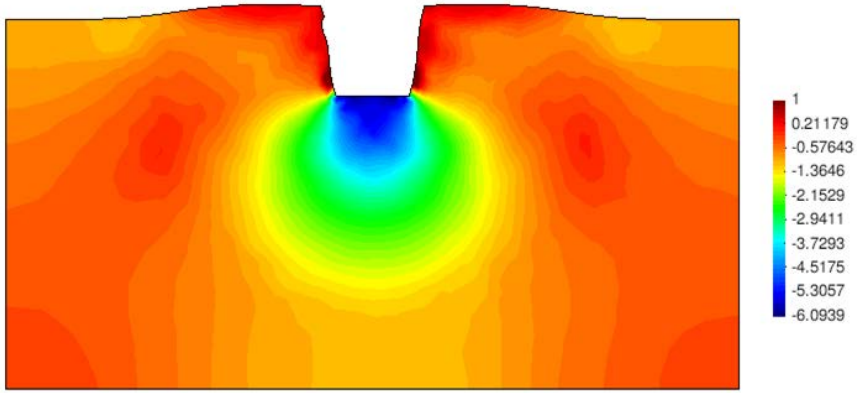

J2

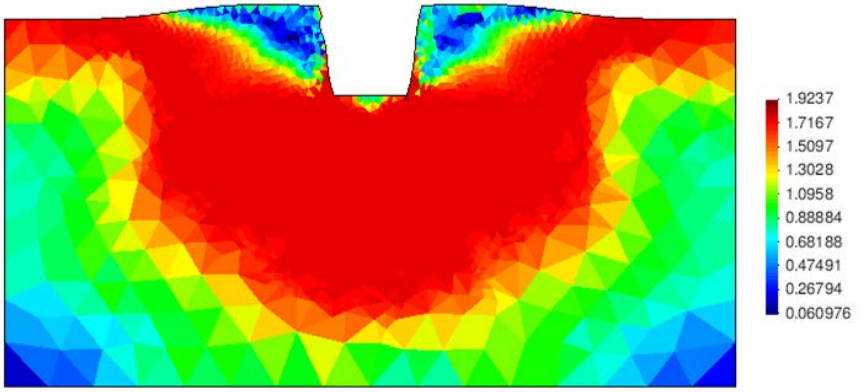

***u*-*p* formulation**

Total mean stress

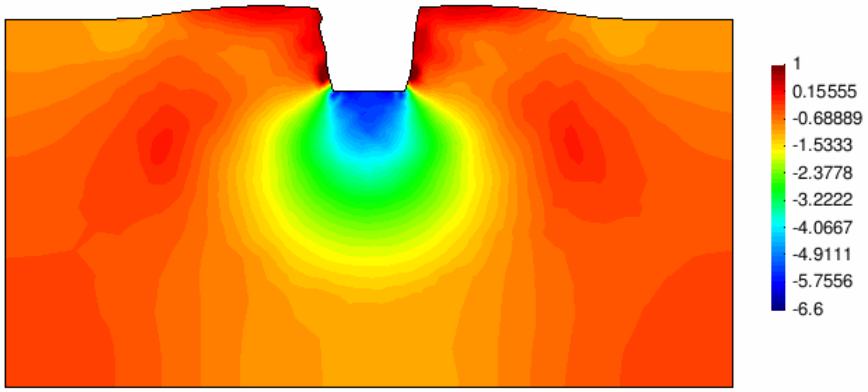

Incremental plastic shear strain

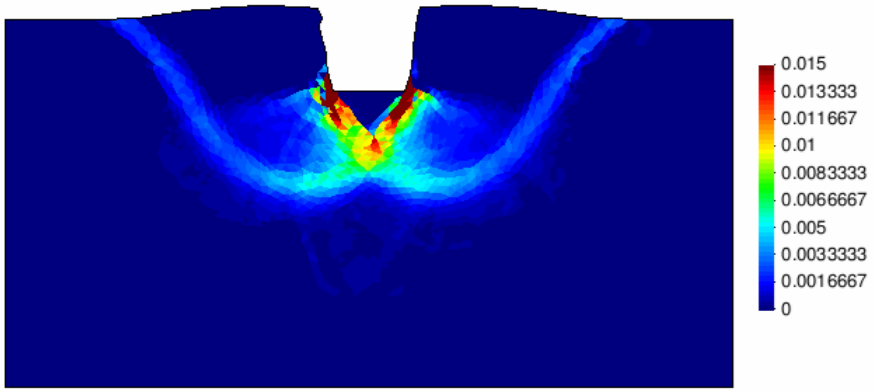

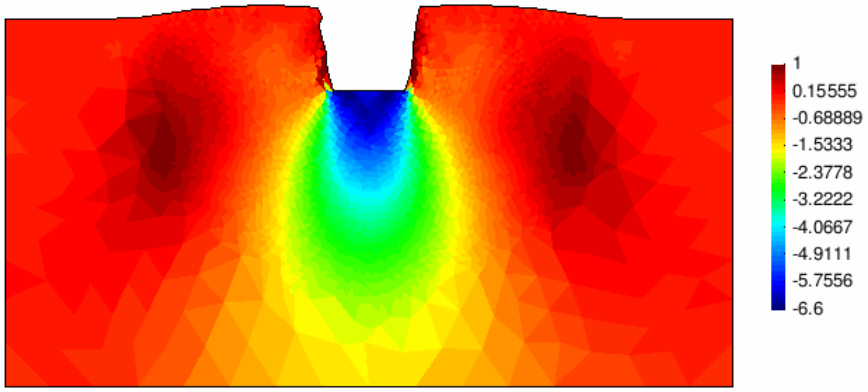

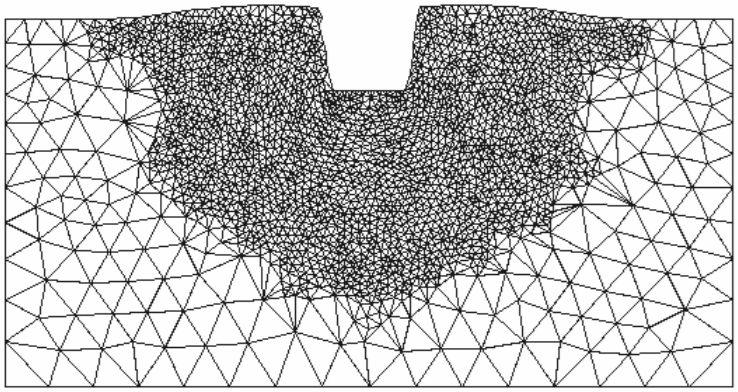

Total vertical stress

Case	Formulation	Mapping	Initial Mesh	Initial number of elements	Final number of elements
PFEM_F_1	Displacement (u-only)	Centroid	Coarse	14,427	14,556
PFEM_F_2	Mixed stabilized (u-p)	Centroid	Coarse	14,427	14,601
PFEM_F_3	Mixed stabilized (u-p)	Centroid	X-Coarse	1669	4669
PFEM_F_4	Mixed stabilized (u-p)	Least Square	X-Coarse	1669	4977
PFEM_F_5	Mixed stabilized (u-p)	Centroid	Half X-Coarse	832	2551

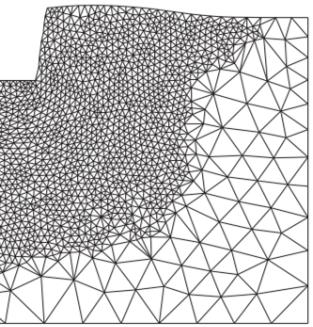

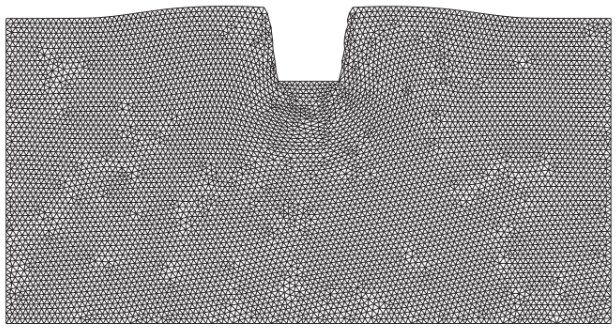

(c) PFEM_F_2

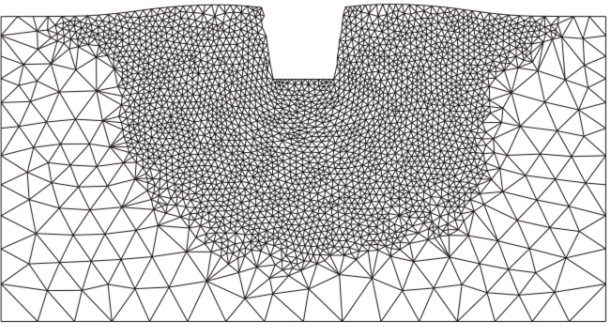

(d) PFEM_F_4

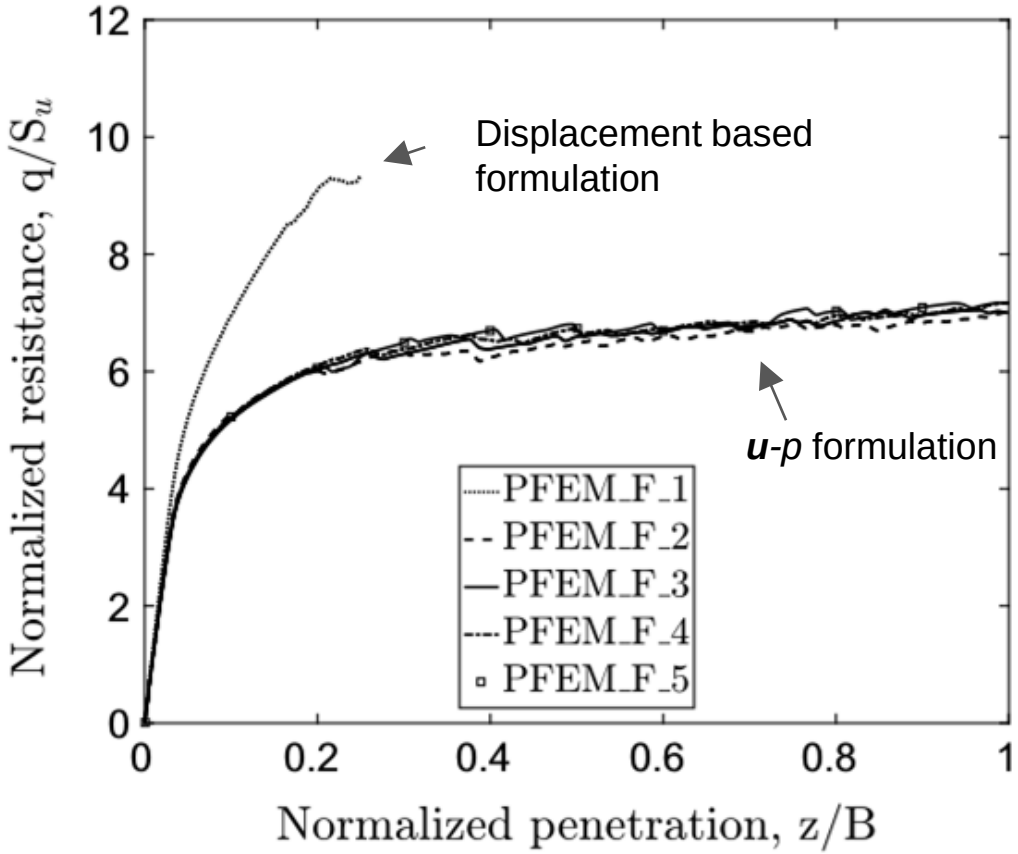

(Kardani et al, 2014)

The same problem (considering the symmetry of the solution) has been solved by Kardani et al (2014) using EALE (Efficient Arbitrary Lagrangian-Eulerian).

In their work, a displacement-based formulation is used in conjunction of high order elements.

Two FE meshes are used: 3700 nodes (coarse) and 14600 nodes (fine).

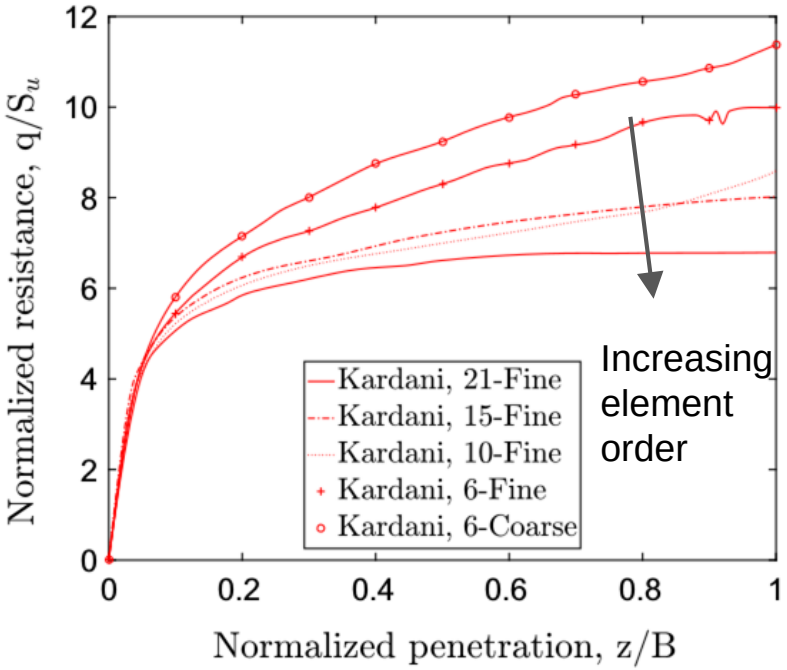

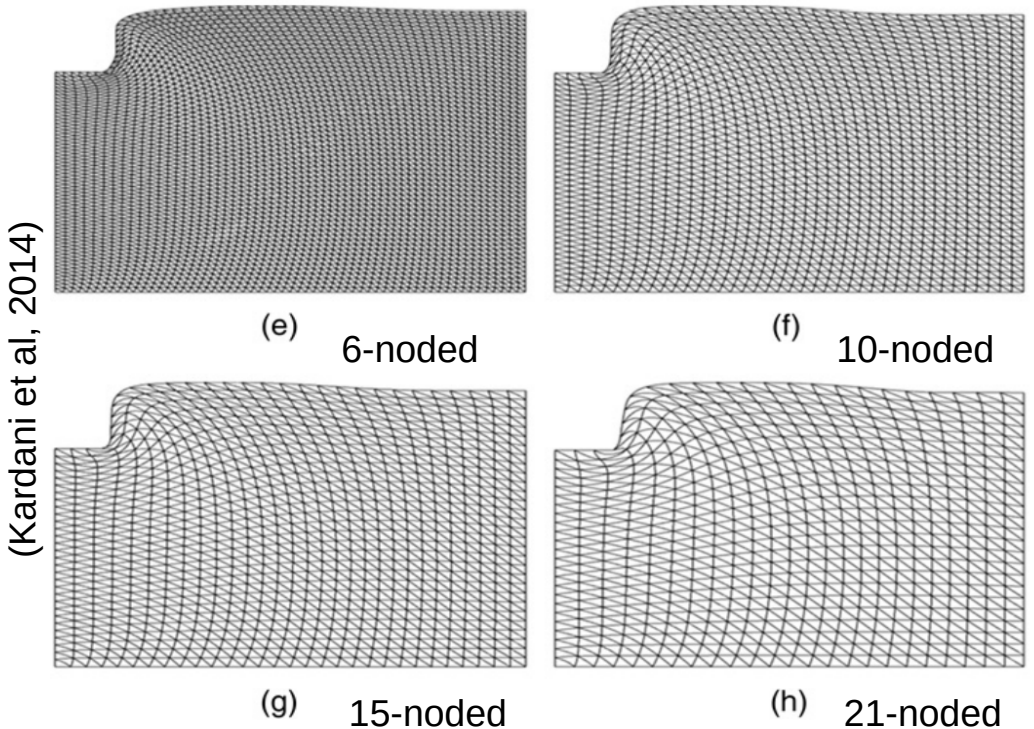

Strip footing on clay

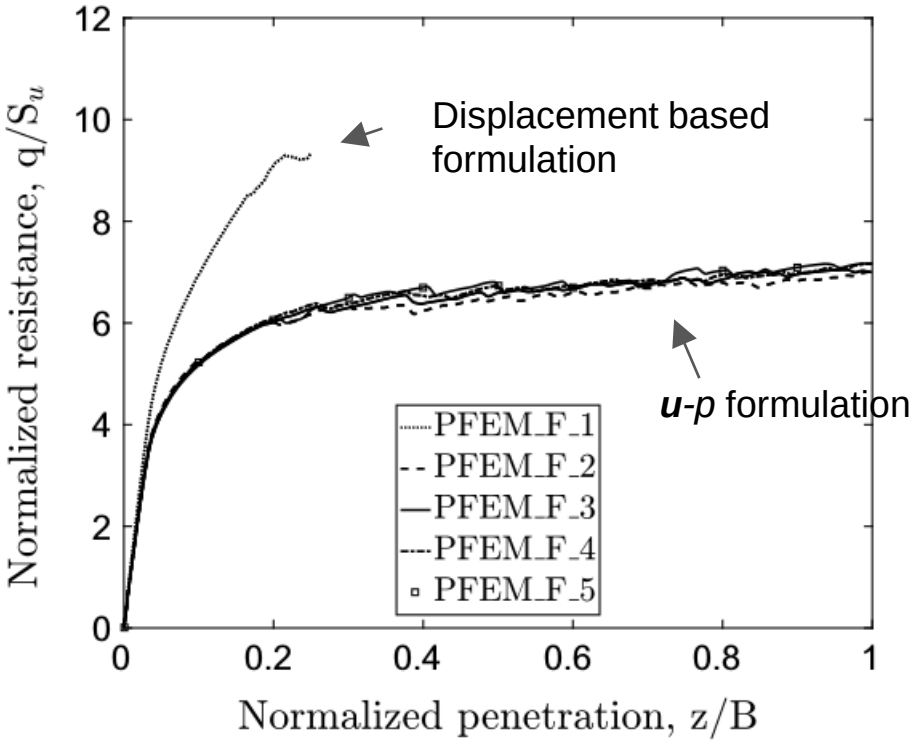

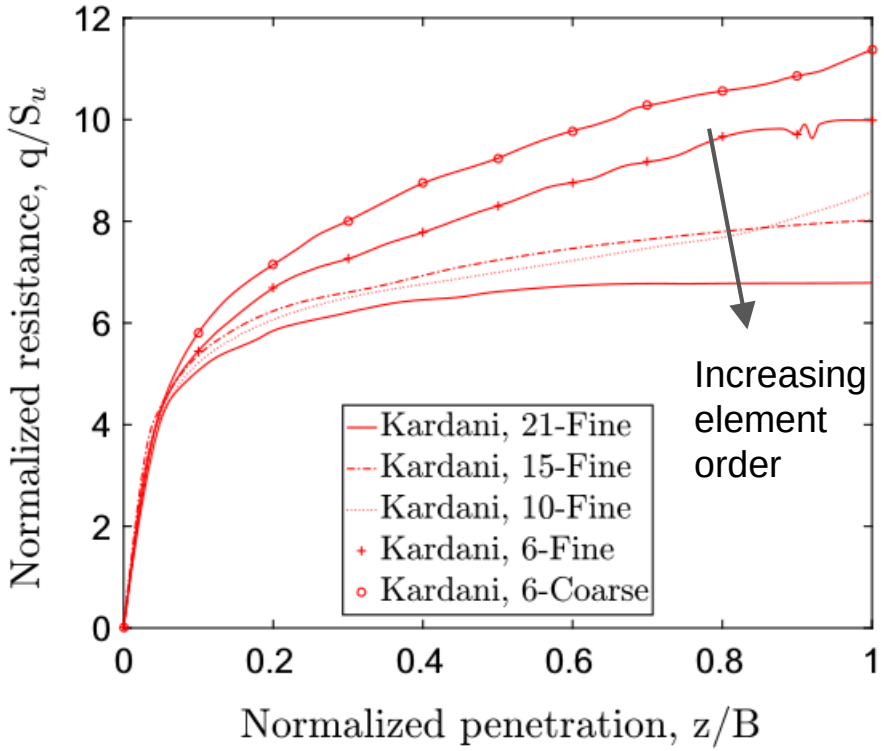

- Thanks to the use of a mixed-stabilized formulation and *h*-adaptive methods, a similar accuracy is obtained with only 14% of DoF and GP.

Case	Elements	Interp. order	Degrees of freedom		Gauss points		N_c
			Initial	Final	Initial	Final	($z/B = 1$)
PFEM_F_5	3-noded triangle	1	1371	3978	832	2551	7.16
EALE-6-Coarse	6-noded	2	7442	7442	10,800	10,800	11.38
EALE-6-Fine	6-noded	2	29,282	29,282	43,200	43,200	9.99
EALE-10-Fine	10-noded	3	29,282	29,282	19,200	19,200	8.59
EALE-15-Fine	15-noded	4	29,282	29,282	21,600	21,600	8.02
EALE-21-Fine	21-noded	5	29,282	29,282	18,432	18,432	6.73

Comparison of the mixed forms

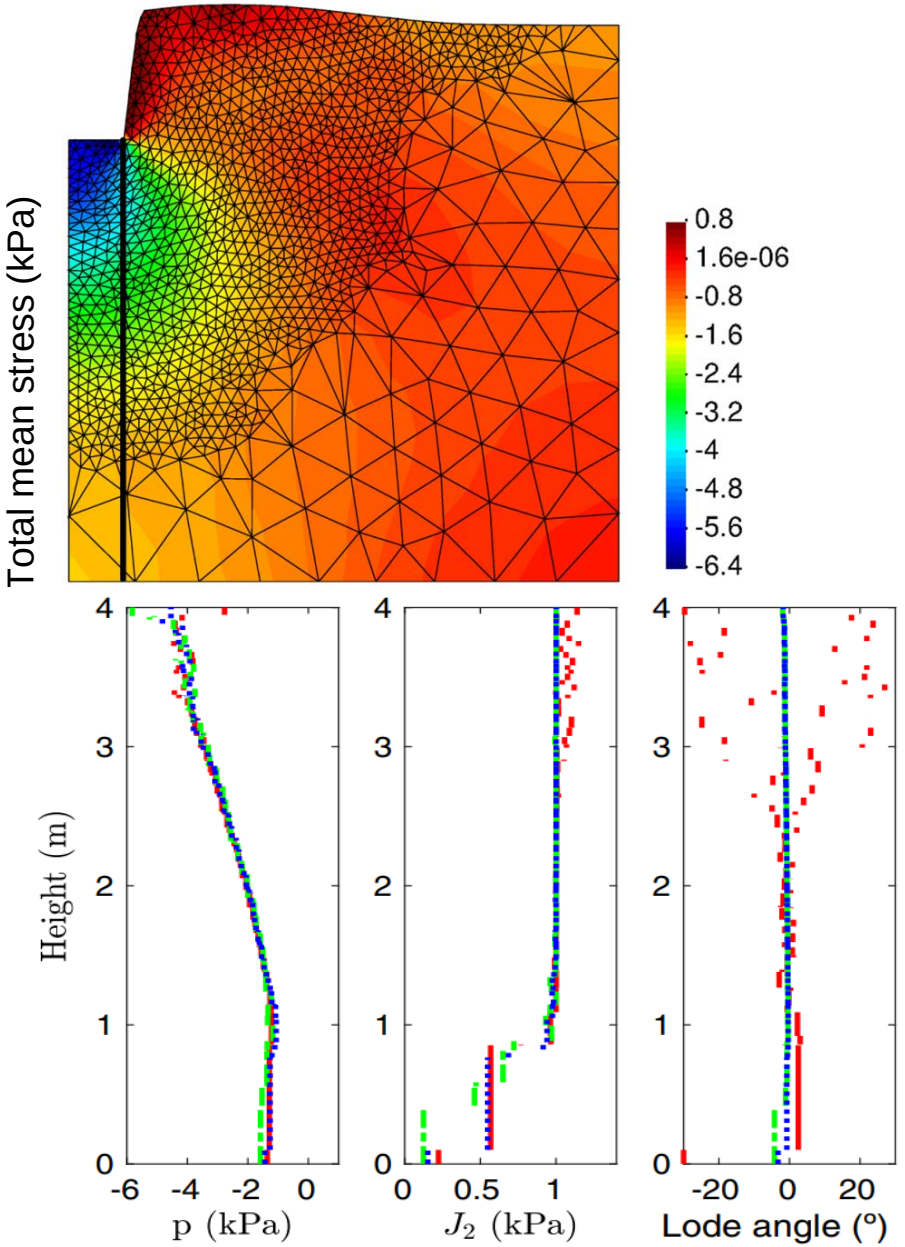

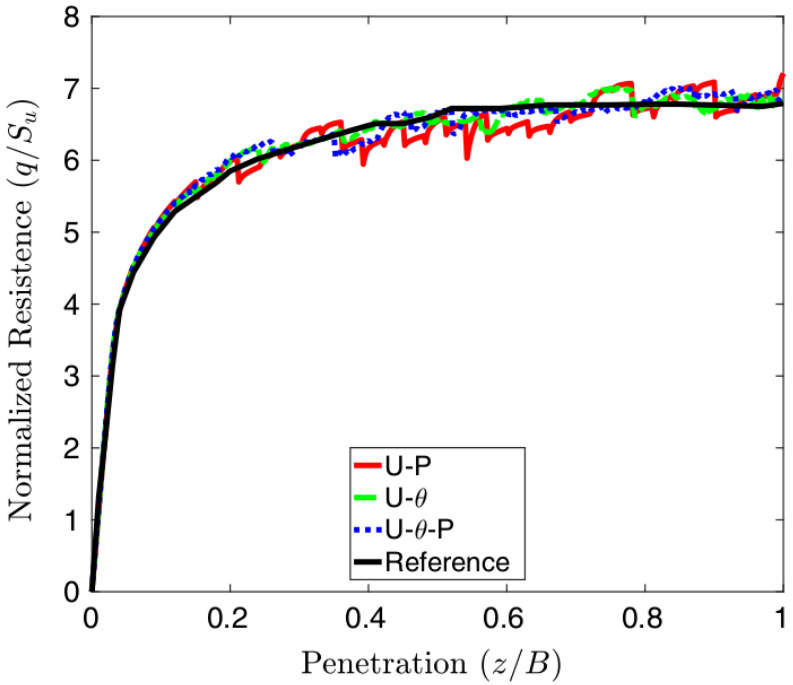

A similar load-displacement curve is obtained irrespectively of the mixed formulation.

However, differences are more visible in vertical profiles of the stress invariants: using the ***u-p*** formulation the Lode angle presents spurious oscillations in the upper part.

Origin of the oscillations

One of the causes of the sudden drops of resistance in the load-displacement curves are due to the insertion of new nodes in the contour.

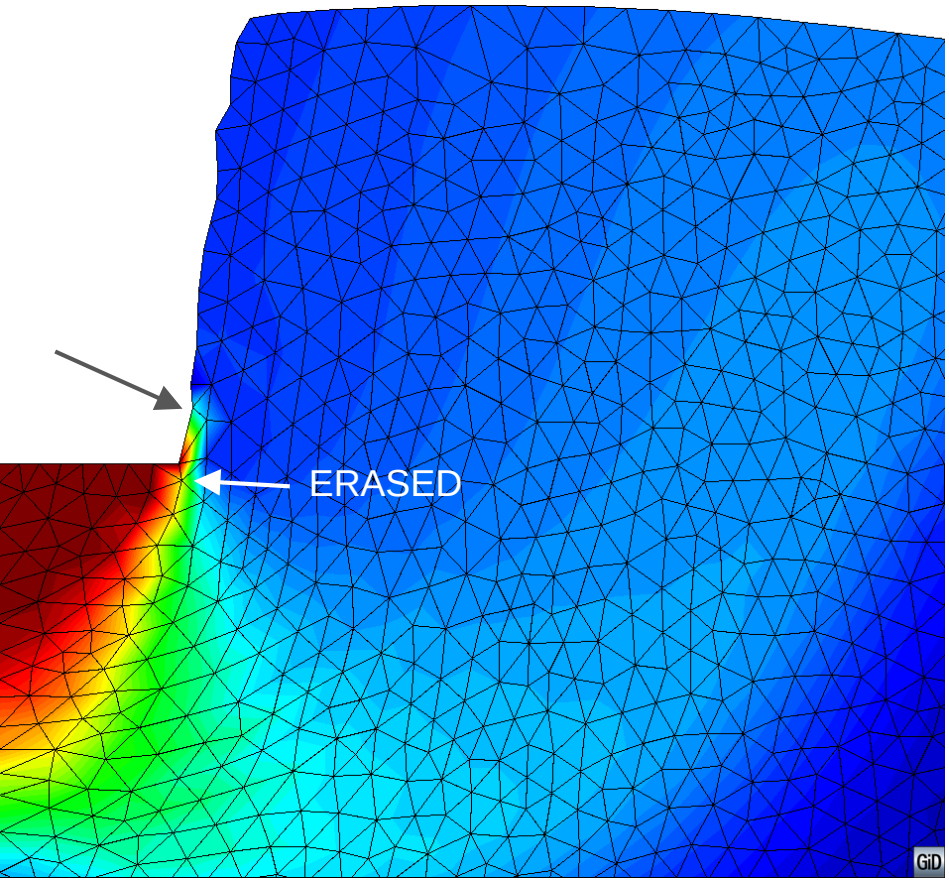

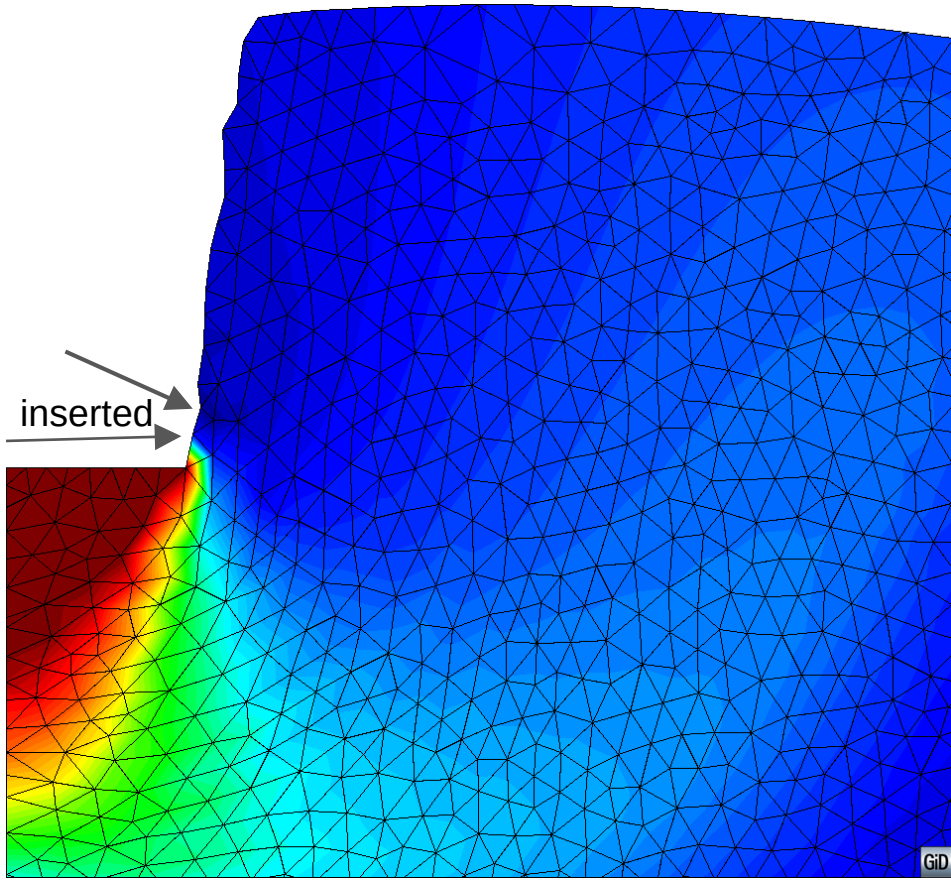

Velocity contours at two consecutive time-steps.

Comparison of the mixed forms

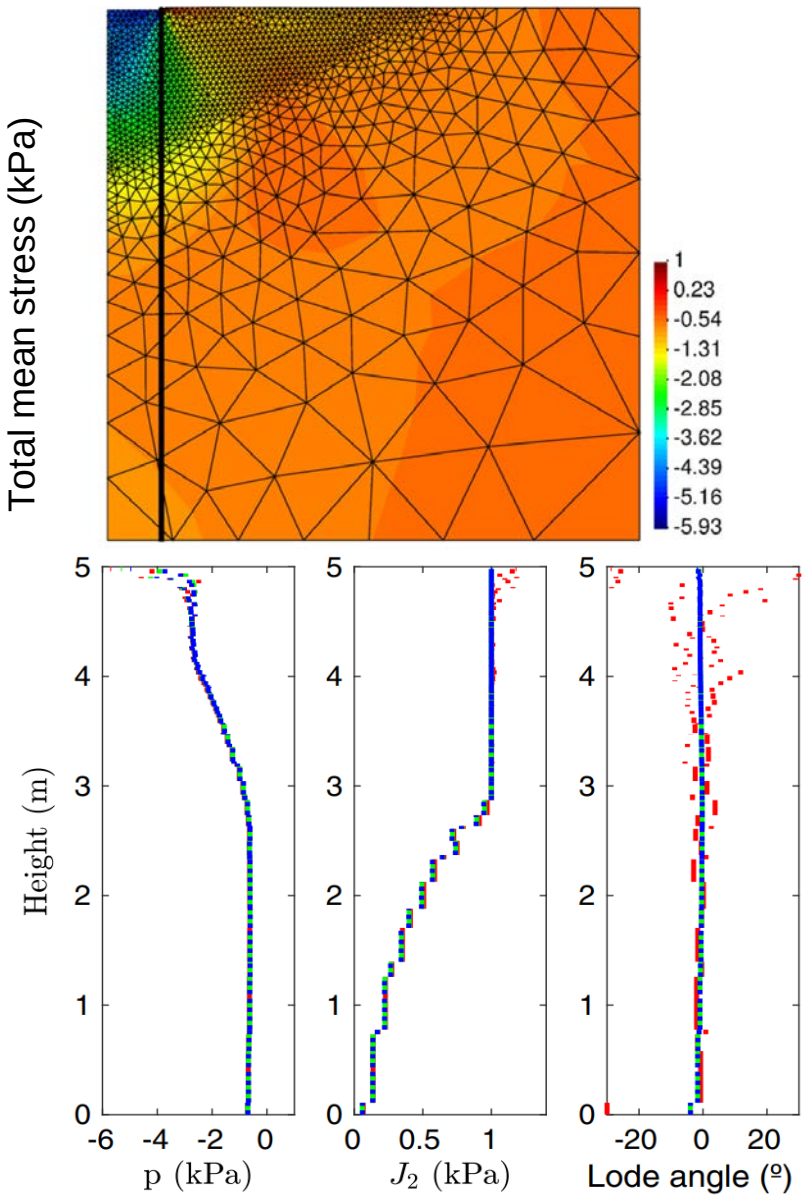

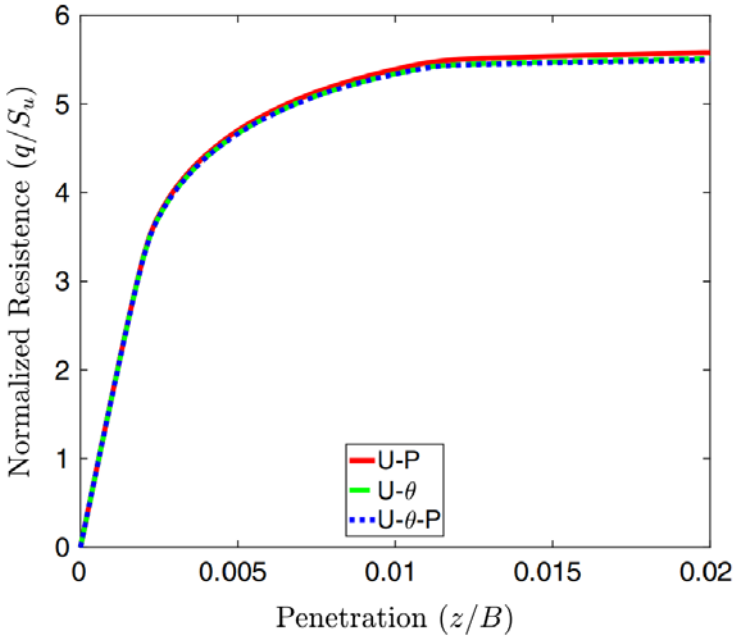

The problem is recomputed using a much higher Rigidiy index: $I_r = G/S_u = 500$.

As failure is reached at lower displacements, no remeshing is applied.

The same suprious oscillations in the Lode angle are found using the ***u-p*** formulation.

Mixed forms for the hydro-mechanical problem

- Compressible constitutive equations are used for the solid skeleton.
  - However, Critical state theory also predicts zero volume change at critical state.
- The mixture behaves like an incompressible material in almost undrained conditions (i.e. rapid application of loads with respect to the permeability).
- Low order elements tend to present highly oscillatory pressure fields.

To this end, the following stabilized mixed forms are used:

***u*-*J*-p_w**

$$\begin{cases} \nabla \cdot (\breve{\boldsymbol{\sigma}}' + p_w \mathbb{1}) + \mathbf{b} = \mathbf{0} \\ J - \theta = 0 \\ \dfrac{-1}{\kappa_w} \dot{p}_w + \dfrac{\dot{\theta}}{\theta} + \nabla \cdot \mathbf{v}^d = 0 \end{cases}$$

***u*-*p'*-p_w**

$$\begin{cases} \nabla \cdot (\mathrm{dev}(\boldsymbol{\sigma}') + p' \mathbb{1} + p_w \mathbb{1}) + \mathbf{b} = \mathbf{0} \\ p' - (\frac{1}{3}\mathbb{1} : \boldsymbol{\sigma}') = 0 \\ \dfrac{-1}{\kappa_w} \dot{p}_w + \nabla \cdot \mathbf{v} + \nabla \cdot \mathbf{v}^d = 0 \end{cases}$$

where:

$$\breve{\boldsymbol{\sigma}} = \hat{\boldsymbol{\sigma}}(\breve{\boldsymbol{F}}, V)$$

$$\breve{\mathbf{F}} = \mathbf{F}^v \mathbf{F}^d = (\theta^{\frac{1}{3}})(\det(\mathbf{F})^{-\frac{1}{3}} \mathbf{F}) = \left(\frac{\theta}{\det(\mathbf{F})} \right)^{\frac{1}{3}} \mathbf{F}$$

A stabilization term, PPP, is added to the Jacobian and effective pressure equations; whereas the mass conservation equation is stabilized by the Fluid Pressure Laplacian (FPL) technique.

Mixed forms for the hydro-mechanical problem

***u*-*J*-p_w**

$$\begin{cases} \mathbf{P}(\breve{\boldsymbol{\sigma}}') + \mathbf{Q} \cdot \tilde{\mathbf{p}}_{\mathrm{w}} = \mathbf{f}^{\mathrm{ext}} \\ \left(\mathbf{M} + \dfrac{\alpha_{\mathrm{s}}^{\theta}}{\mu}\mathbf{M}^{s}\right) \cdot \tilde{\theta} = \mathbf{f}^{\theta} \\ \mathbf{M}^{\star} \cdot \dot{\tilde{\theta}} - \left(\mathbf{H}^{s} + \dfrac{1}{\kappa_{\mathrm{w}}}\mathbf{M}\right) \cdot \dot{\tilde{\mathbf{p}}}_{\mathrm{w}} - \mathbf{H} \cdot \tilde{\mathbf{p}}_{\mathrm{w}} = \mathbf{f}^{p_{\mathrm{w}}} \end{cases}$$

***u*-*p*'-p_w**

$$\begin{cases} \mathbf{P}(\mathrm{dev}(\boldsymbol{\sigma}')) + \mathbf{Q} \cdot \tilde{\mathbf{p}}' + \mathbf{Q} \cdot \tilde{\mathbf{p}}_{\mathrm{w}} = \mathbf{f}^{\mathrm{ext}} \\ \left(\mathbf{M} + \dfrac{\alpha_{\mathrm{s}}^{p}}{\mu}\mathbf{M}^{s}\right) \cdot \tilde{\mathbf{p}}' = \mathbf{f}^{p}(\boldsymbol{\sigma}') \\ \mathbf{Q}^{\star T} \cdot \dot{\tilde{\mathbf{u}}} - \left(\mathbf{H}^{s} + \dfrac{1}{\kappa_{\mathrm{w}}}\mathbf{M}\right) \cdot \dot{\tilde{\mathbf{p}}}_{\mathrm{w}} - \mathbf{H} \cdot \tilde{\mathbf{p}}_{\mathrm{w}} = \mathbf{f}^{p_{\mathrm{w}}} \end{cases}$$

$$\mathbf{P}(\boldsymbol{\sigma}) = \int_{\Omega_t} \mathbf{B}^T \cdot \underline{\boldsymbol{\sigma}} \, \mathrm{d}\Omega_t$$

$$\mathbf{Q} = \int_{\Omega_t} \mathbf{B}^T \cdot \underline{\mathbb{1}} \cdot \mathbf{N} \, \mathrm{d}\Omega_t$$

$$\mathbf{M}^{s} = \int_{\Omega_t} \mathbf{N}^T \cdot \mathbf{N} \frac{1}{J} \, \mathrm{d}\Omega_t - \int_{\Omega_t} \breve{\mathbf{N}}^T \cdot \breve{\mathbf{N}} \frac{1}{J} \, \mathrm{d}\Omega_t$$

$$\mathbf{M} = \int_{\Omega_t} \mathbf{N}^T \cdot \mathbf{N} \frac{1}{J} \, \mathrm{d}\Omega_t$$

$$\mathbf{f}^{\mathrm{ext}} = \int_{\Omega_t} \mathbf{N}_u^T \cdot \mathbf{b} \, \mathrm{d}\Omega_t + \int_{\Gamma_{\bar{t}}} \mathbf{N}_u^T \cdot \bar{\mathbf{t}} \, \mathrm{d}\Gamma$$

$$\mathbf{f}^{\theta} = \int_{\Omega_t} \mathbf{N}^T \, d\Omega_t$$

$$\mathbf{f}^{p}(\boldsymbol{\sigma}) = \int_{\Omega_t} \mathbf{N}^T \left(\frac{1}{3}\mathbb{1} : \boldsymbol{\sigma}\right) \frac{1}{J} \, \mathrm{d}\Omega_t$$

$$\mathbf{Q}^{\star T} = \int_{\Omega_t} \mathbf{N}^T \cdot \underline{\mathbb{1}} \cdot \mathbf{B} \frac{1}{J} \, \mathrm{d}\Omega_t$$

$$\mathbf{H} = \int_{\Omega_t} (\nabla \mathbf{N})^T \cdot \mathbf{k}_{\mathrm{p}} \cdot (\nabla \mathbf{N}) \frac{1}{J} \, \mathrm{d}\Omega_t$$

$$\mathbf{f}^{p_{\mathrm{w}}} = \int_{\Omega t} (\nabla \mathbf{N})^T \cdot \mathbf{k}_{\mathrm{p}} \cdot \mathbf{g} \frac{\rho_{\mathrm{w}}}{J} \, \mathrm{d}\Omega_t + \int_{\Gamma_g} (\nabla \mathbf{N})^T \overline{g} \frac{1}{J} \, \mathrm{d}\Gamma$$

Cone penetration test (CPT)

- The interpretation of CPT (obtain soil constitutive parameters based on measured reactions) is still based on empiricism.
- In the model, axisymmetric conditions are considered.
- K = 10^{-7} m/s; OCR = 1.12

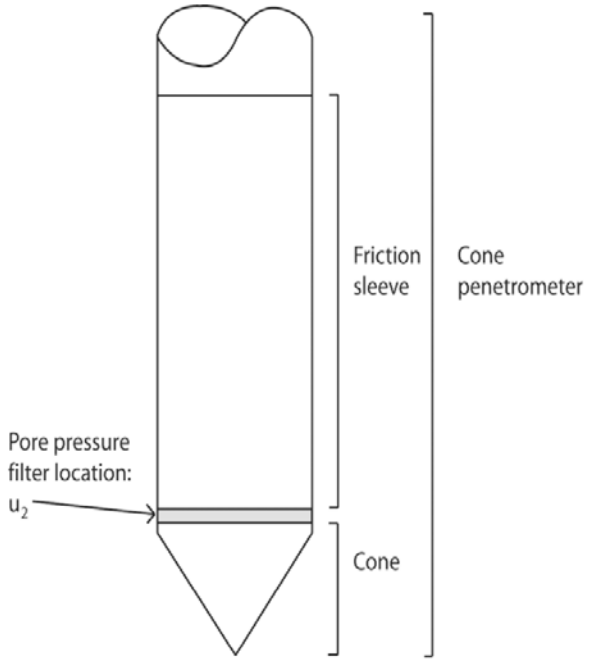

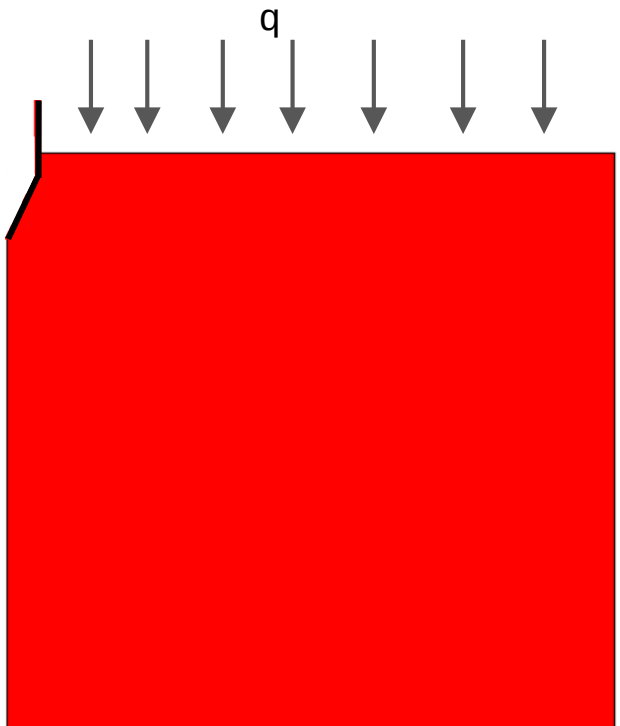

κ^*	λ^*	α	G_0(kPa)	p_0(kPa)
0.016	0.1	23.5	400	10
p_{c0}(kPa)	M	σ'_{v0}(kPa)	σ'_{h0}(kPa)	p_{w0}(kPa)
70	1	57.5	28.9	80

Evolution of water pressure and contact stress at the interface for a smooth case.

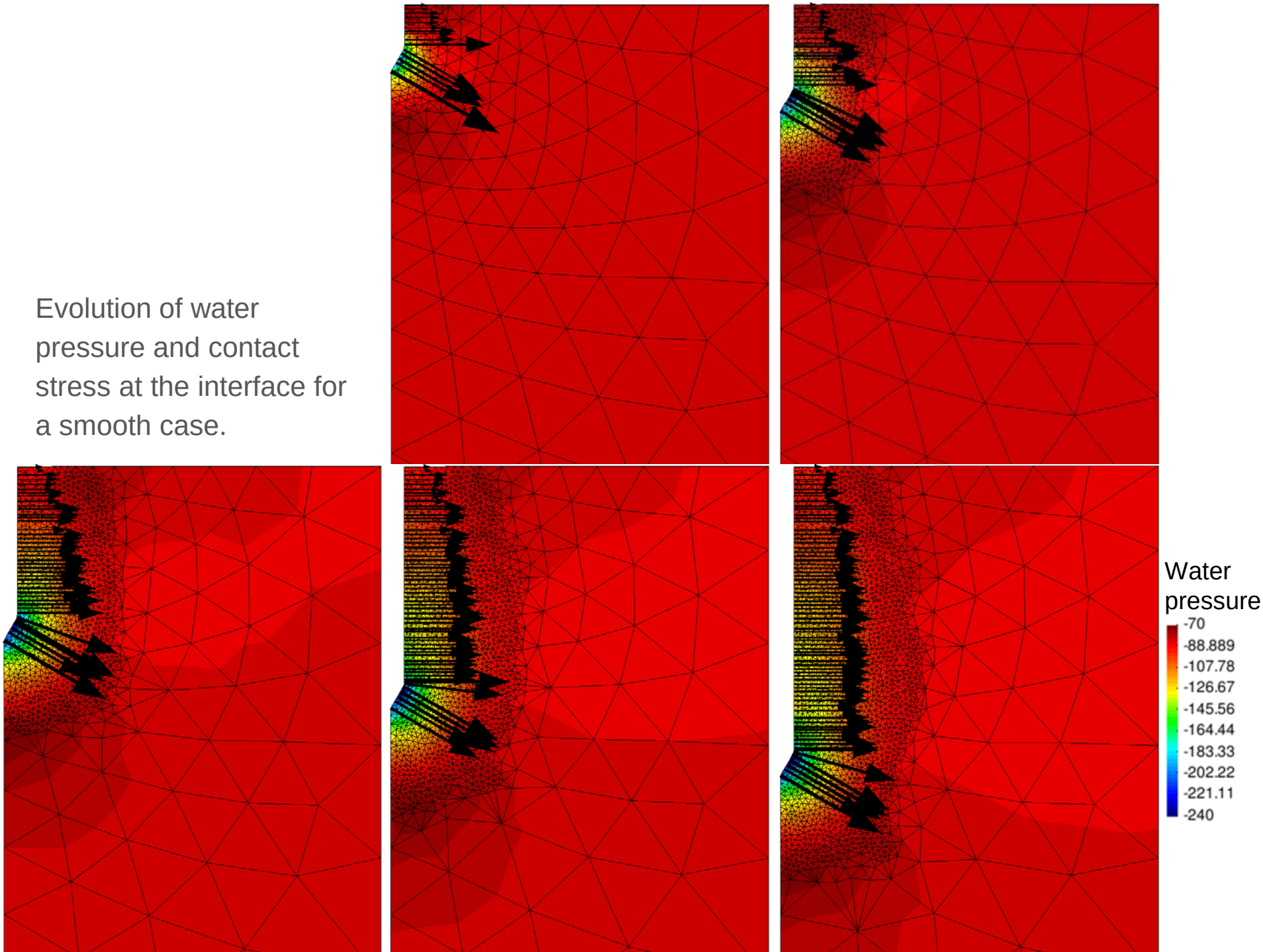

Mixed formulations

The performance of both formulations is compared.

$$\begin{cases} \nabla \cdot \boldsymbol{\sigma} + \mathbf{b} = 0 \\ \dfrac{-1}{\kappa_w}\dot{p}_w + \nabla \cdot \mathbf{v} + \nabla \cdot \mathbf{v}^d = 0 \end{cases} \qquad \begin{cases} \nabla \cdot (\breve{\boldsymbol{\sigma}}' + p_w \mathbb{1}) + \mathbf{b} = 0 \\ J - \theta = 0 \\ \dfrac{-1}{\kappa_w}\dot{p}_w + \nabla \cdot \mathbf{v} + \nabla \cdot \mathbf{v}^d = 0 \end{cases}$$

- Due to the stabilization of the mass conservation equation, both formulations render smooth water pressure profiles.
- The mixed formulation renders smoother load-displacement curve. In fact, the contact stress also present a smoother profile

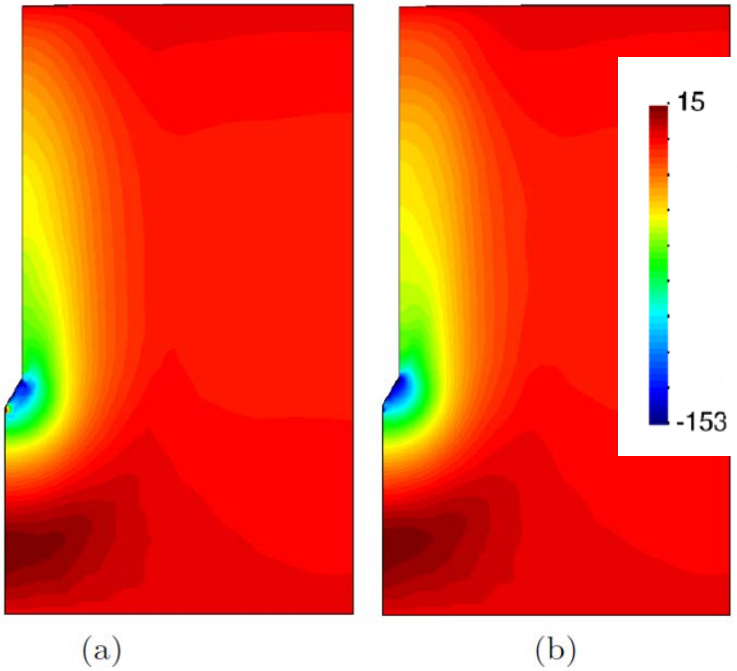

u-p_w u-J-p_w

Water pressure profile:

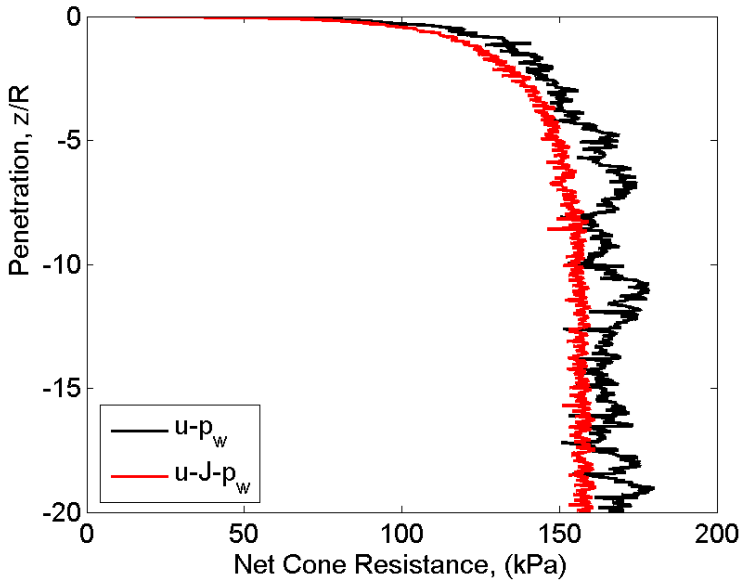

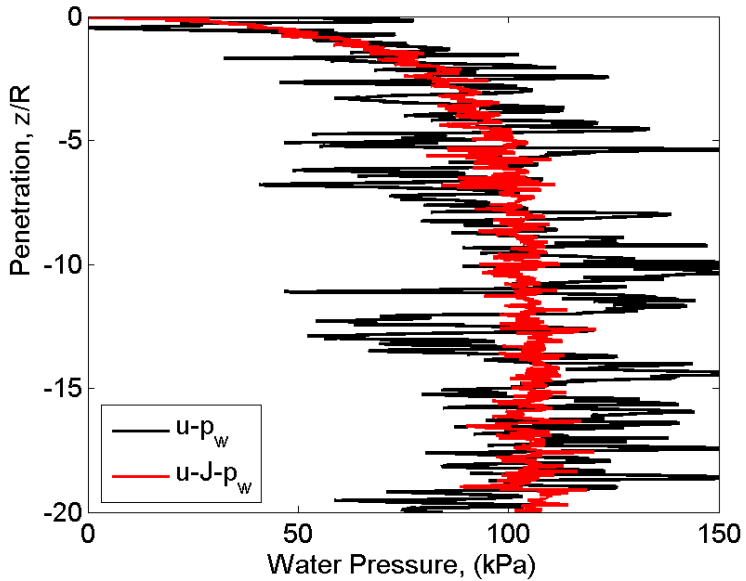

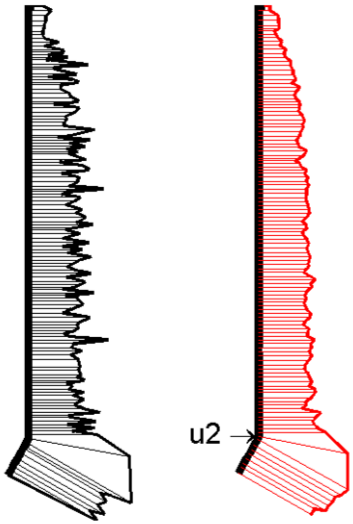

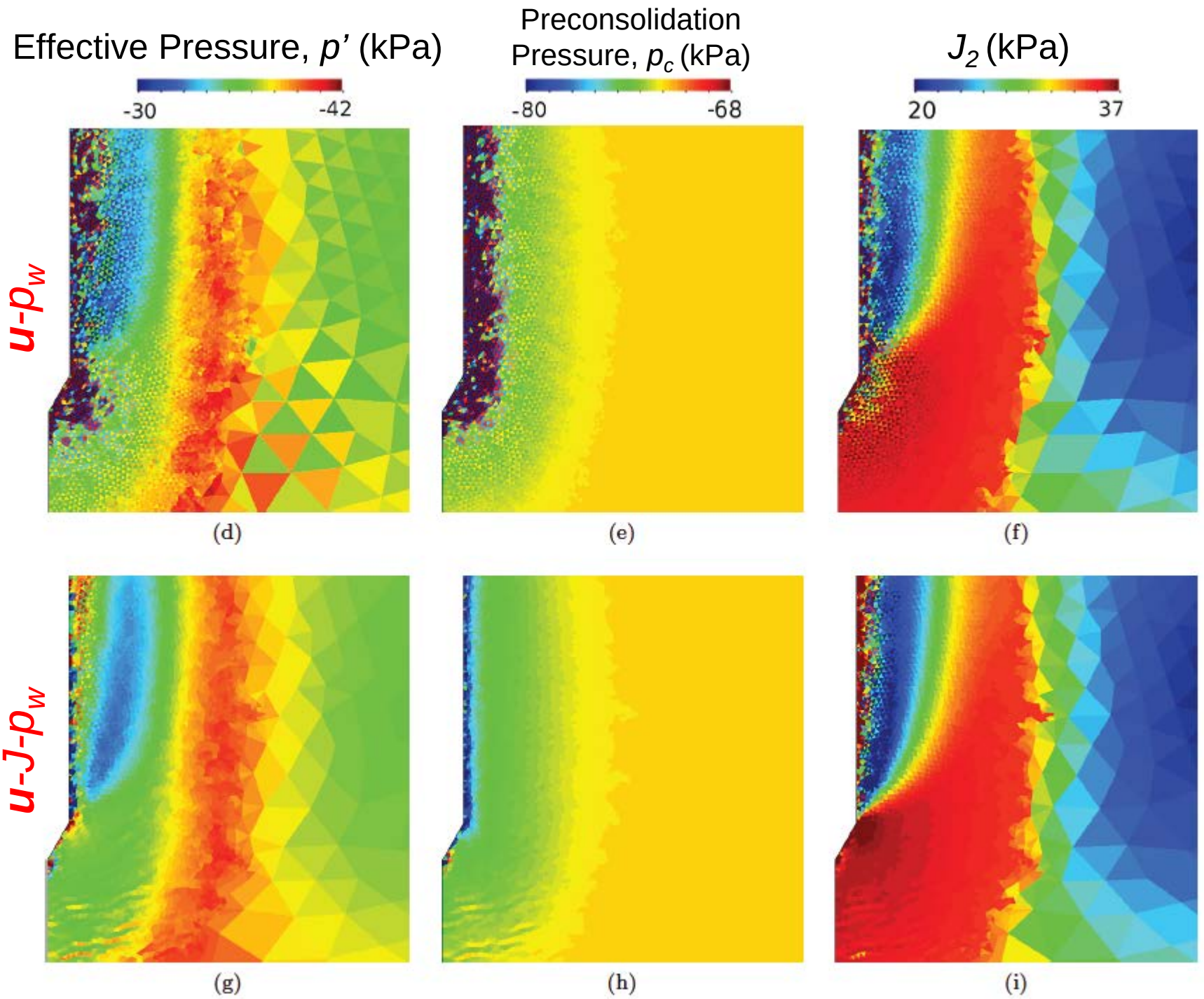
Effective Pressure, p' (kPa)
-30
-42
Preconsolidation Pressure, p_c (kPa)
-80
-68
J_2 (kPa)
20
37
u-p_w
u-J-p_w
(d)
(e)
(f)
(g)
(h)
(i)

Application example

Soil sampler

Sampling can cause significant disturbance so that the samples obtained do not truly reflect the in situ state.

Soil sampler geometry and roughness plays a prominent role in the disturbance of the soil.

It is believed that the vertical strain along the symmetry axis is a good estimator of the sample disturbance.

(Hover et al, 2013)

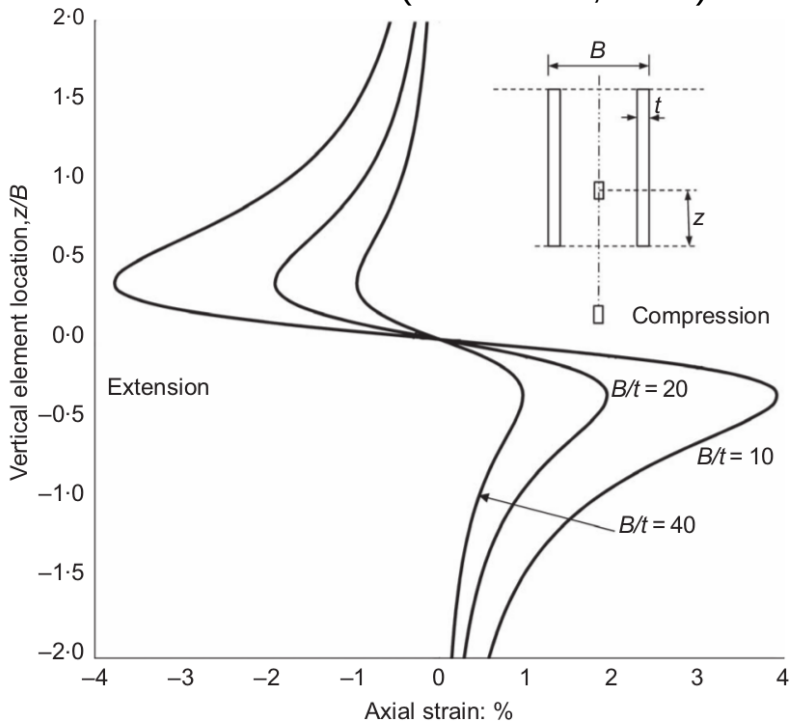

Several cases varying the ratio D/t; the contact roughness and the shape of the cutting edge has been performed.

In all cases the Rigidiy index, $I_r = G/S_u = 100$; $v = 0.49$.

The contact roughness is modelled as:

$$f(\tau) = \tau - \alpha S_u$$

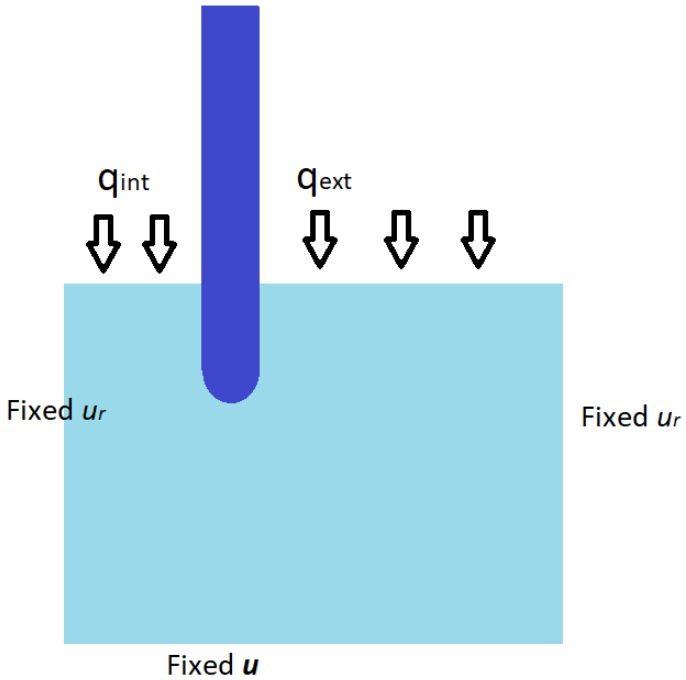

Roud-tipped soil sampler; D/t = 10

Vertical Almansi strain. $\mathbf{e} = \frac{1}{2}\left(\mathbb{1} - \mathbf{F}^{-T} \cdot \mathbf{F}^{-1}\right)$

Smooth interface

Rough interface α = 0.5

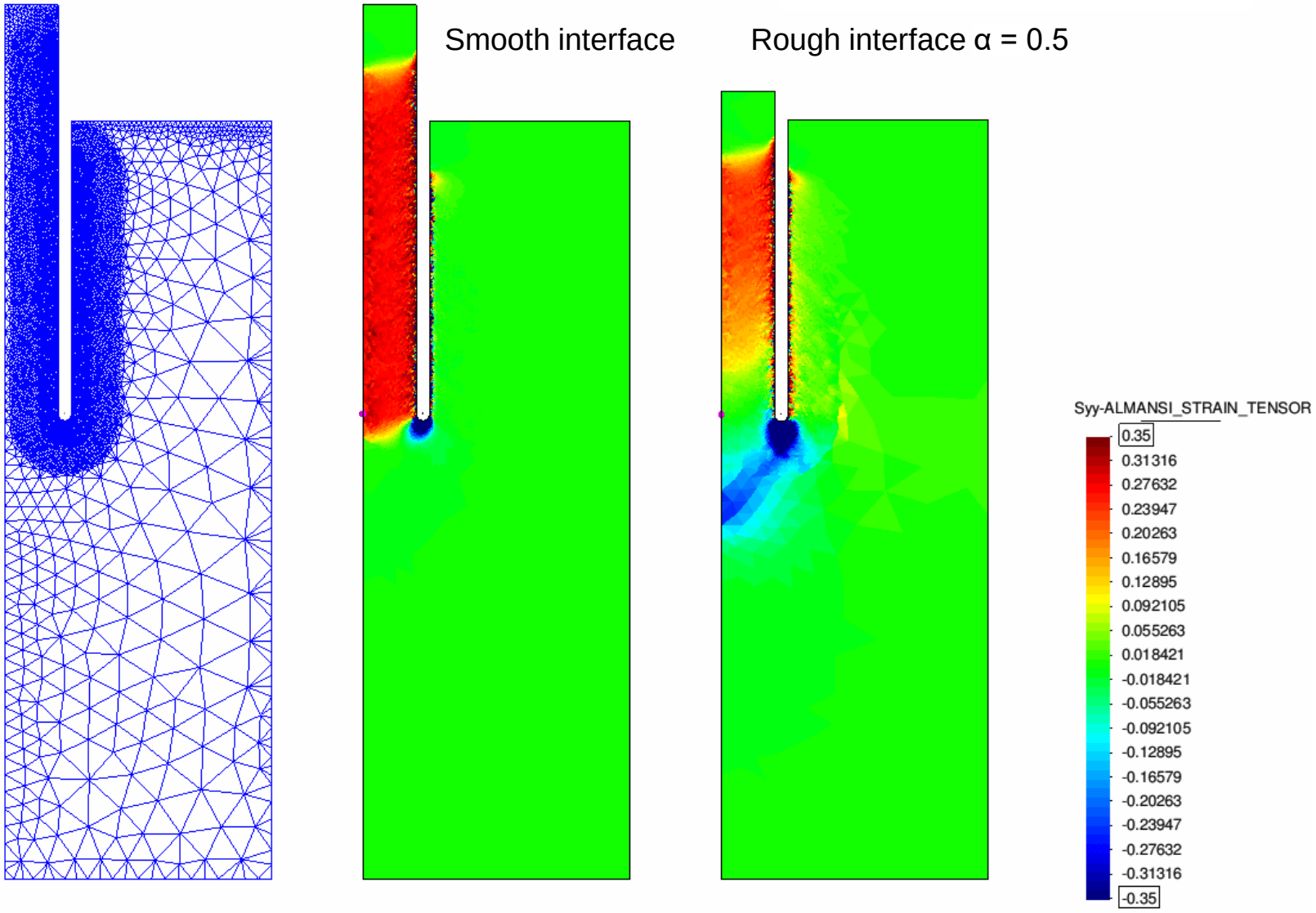

Initial FE mesh: 2413 nodes and 4502 elements.

Final FE mesh: 13568 nodes and 26056 elements.

Round-tip soil sampler; D/t = 10

Smooth interface **Rough interface α = 0.5**

Radial velocity Incremental plastic shear strain Radial velocity

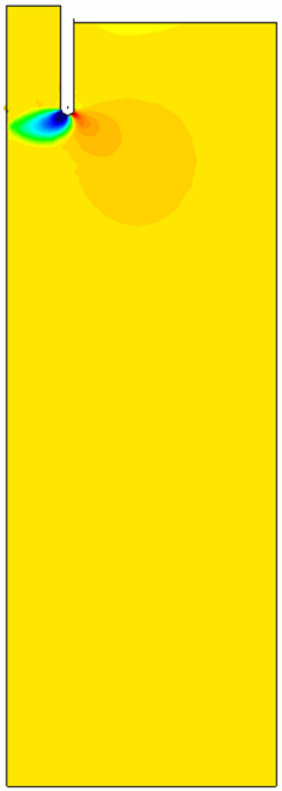

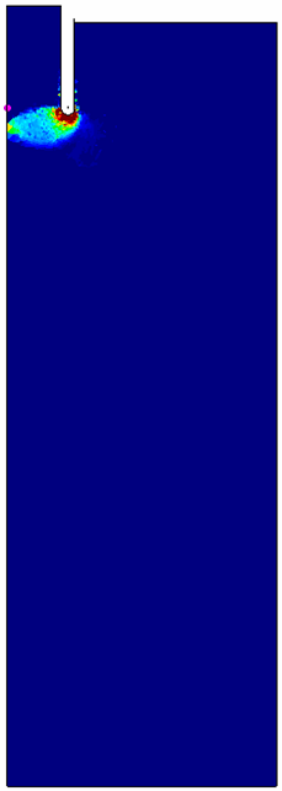

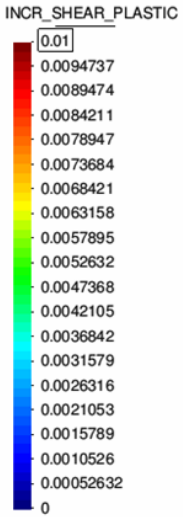

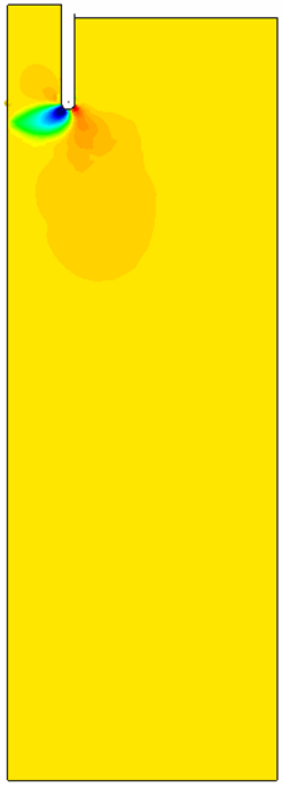

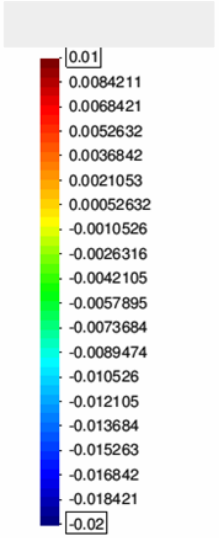

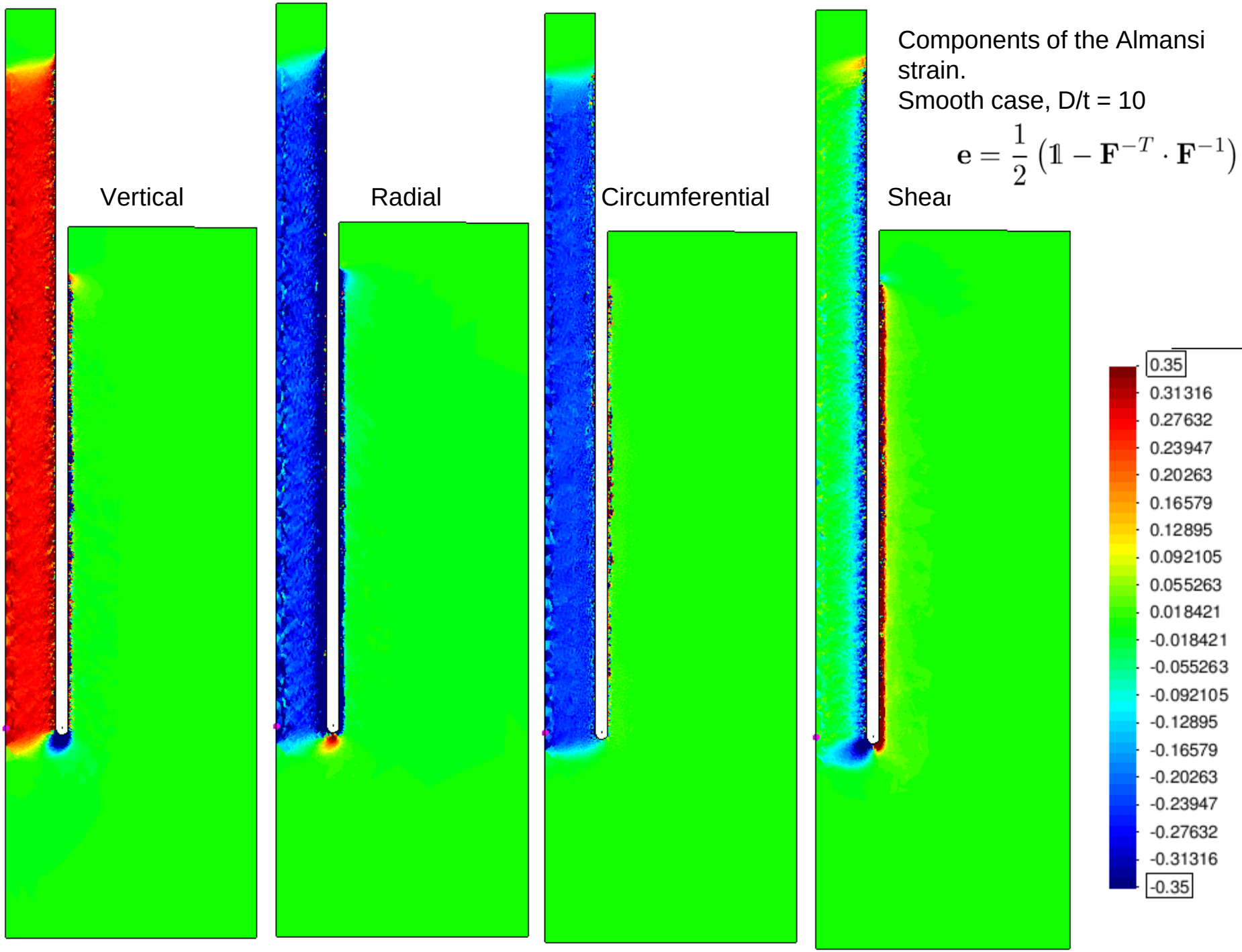
Components of the Almansi strain.
Smooth case, D/t = 10
$$\mathbf{e} = \frac{1}{2}\left(\mathbb{1} - \mathbf{F}^{-T} \cdot \mathbf{F}^{-1}\right)$$
Vertical
Radial
Circumferential
Shear
0.35
0.31316
0.27632
0.23947
0.20263
0.16579
0.12895
0.092105
0.055263
0.018421
-0.018421
-0.055263
-0.092105
-0.12895
-0.16579
-0.20263
-0.23947
-0.27632
-0.31316
-0.35

Components of the Almansi strain.
Rough case, D/t = 10

Vertical

Radial

Circumferential

Shear

$$\mathbf{e} = \frac{1}{2}\left(\mathbb{1} - \mathbf{F}^{-T} \cdot \mathbf{F}\right.$$

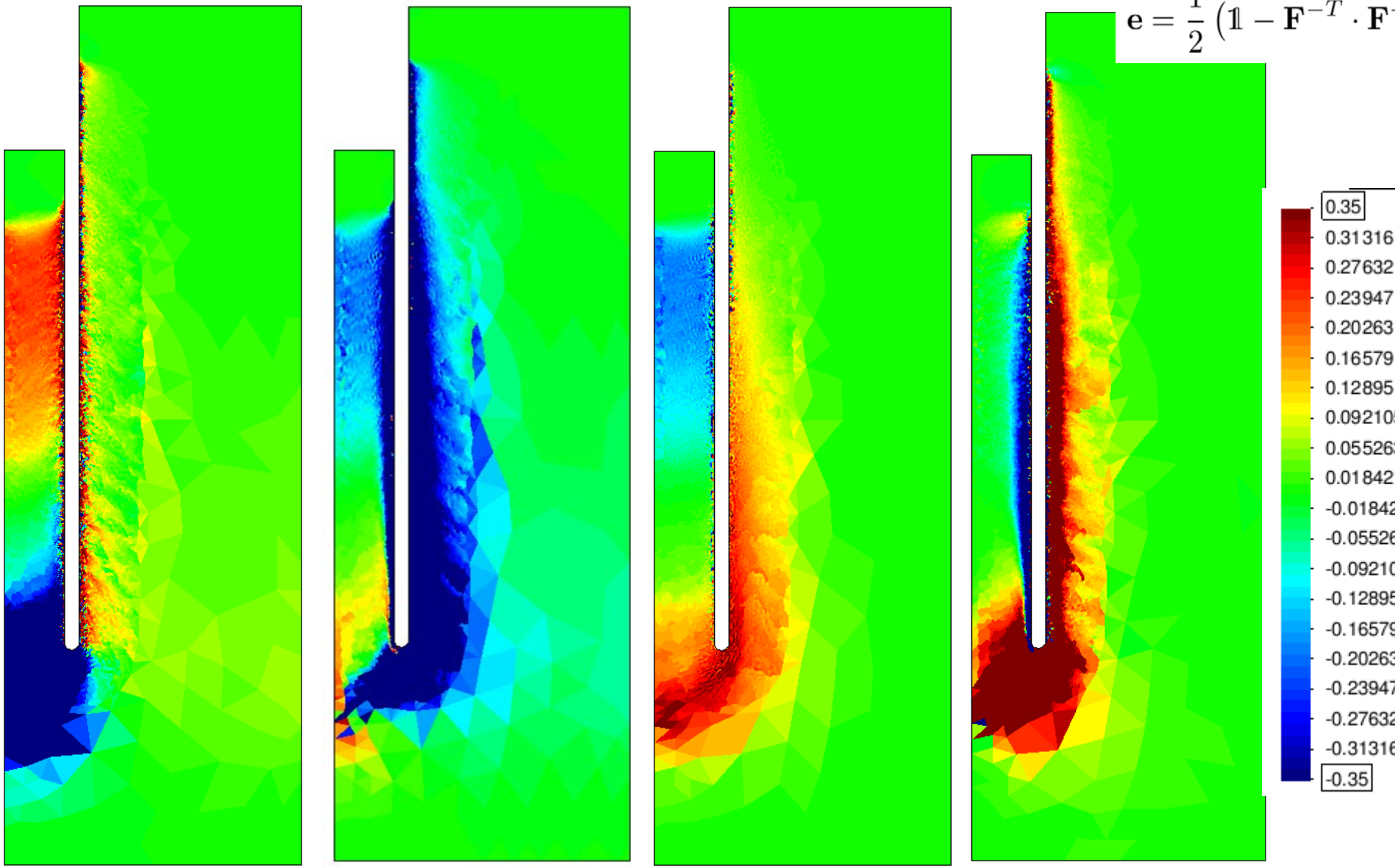

Centreline strain path

Smooth interface

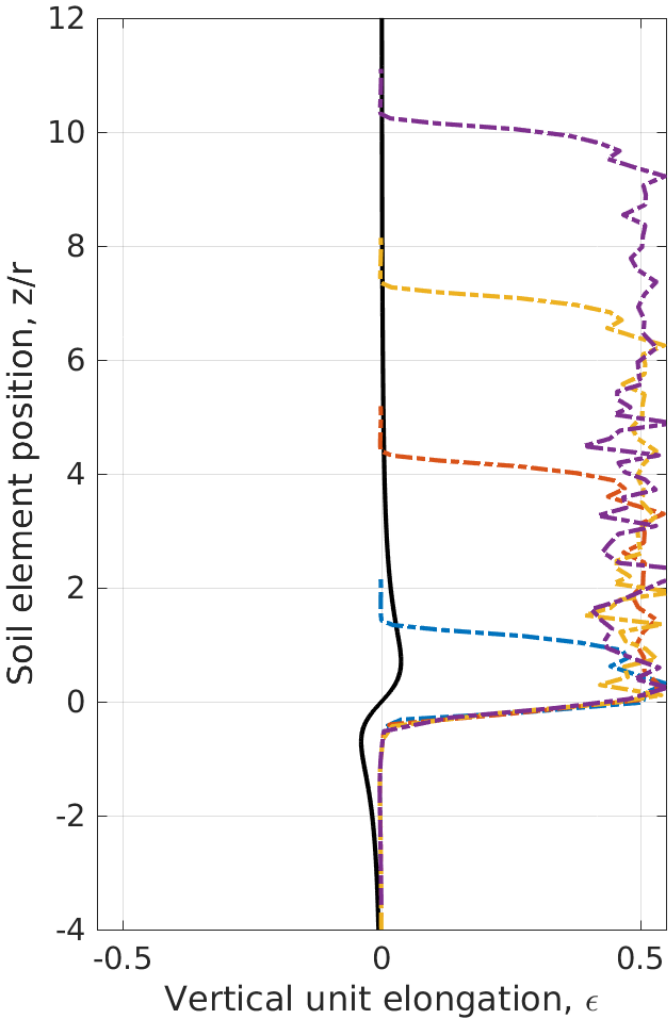

Rough interface α = 0.5

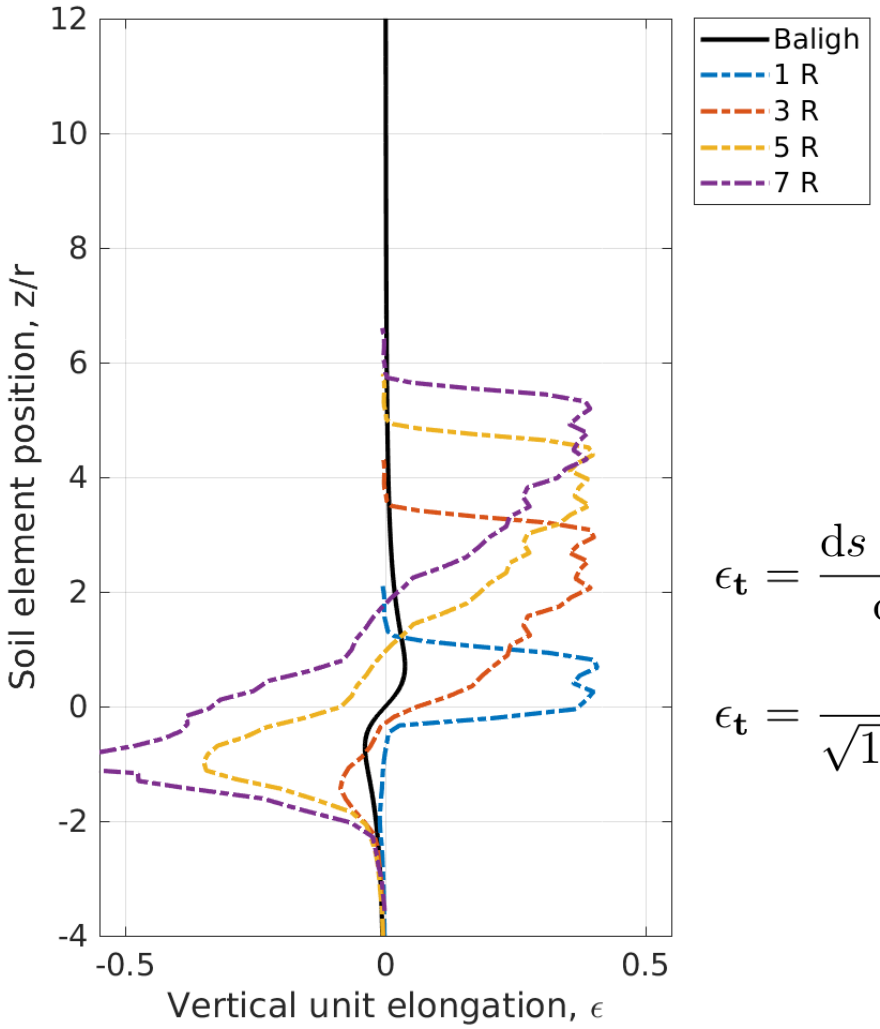

$$\epsilon_{\mathbf{t}} = \frac{\mathrm{d}s - \mathrm{d}S}{\mathrm{d}S} = \mathbf{t} \cdot \boldsymbol{\epsilon} \cdot \mathbf{t}$$

$$\epsilon_{\mathbf{t}} = \frac{1}{\sqrt{1 - 2\,\mathbf{t} \cdot \mathbf{e} \cdot \mathbf{t}}} - 1$$

Specific recovery ratio / Incremental filling ratio

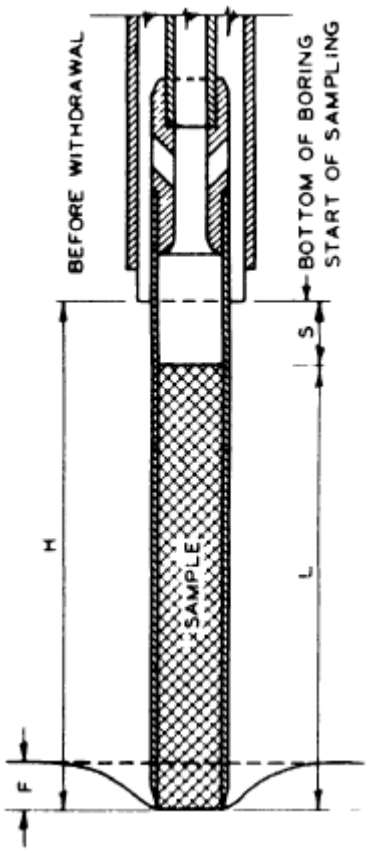

L/H = TOTAL RECOVERY RATIO

ΔL/ΔH = SPECIFIC RECOVERY RATIO

Hvorslev (1949)

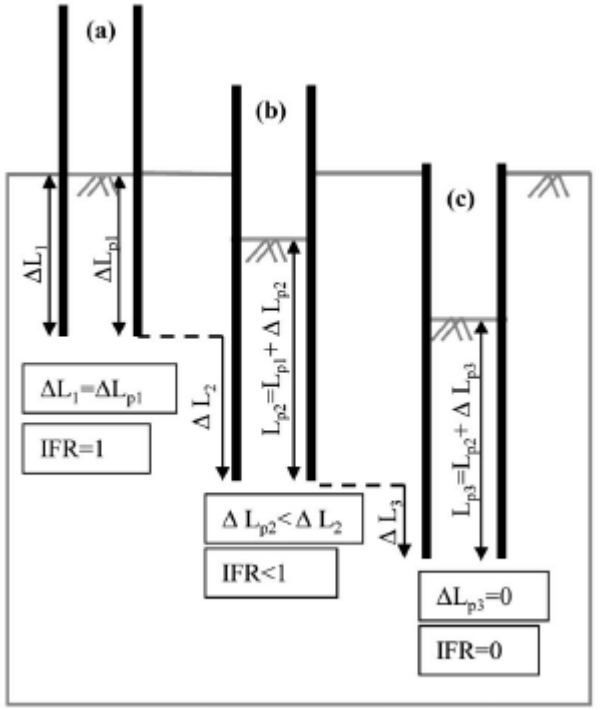

Gavin (2009)

Specific recovery ratio

The specific recovery ratio is defined as the ratio of increment of sample entering the tube to the increment of tube advance.

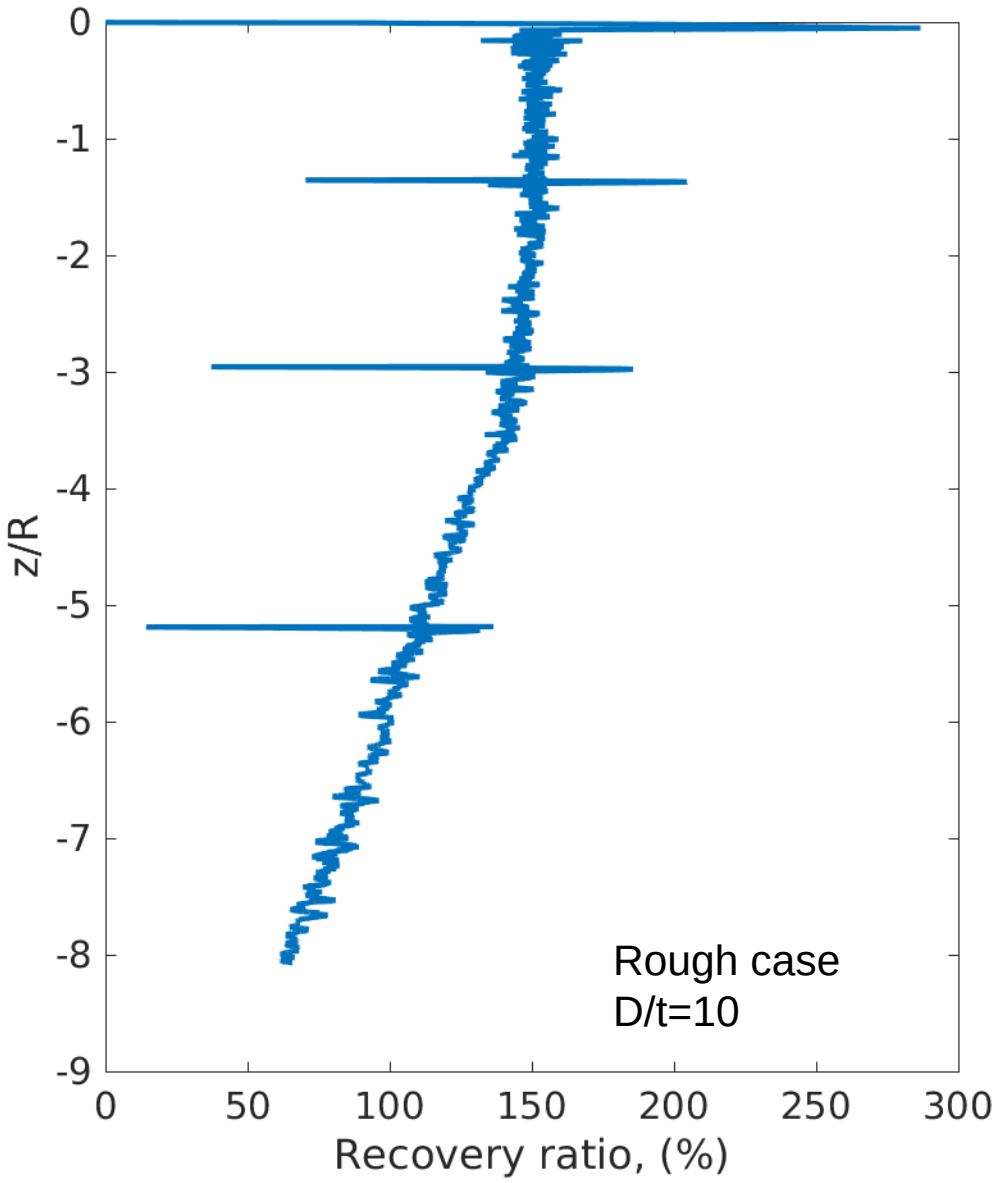

Total mean stress (kPa)

Smooth

Rough

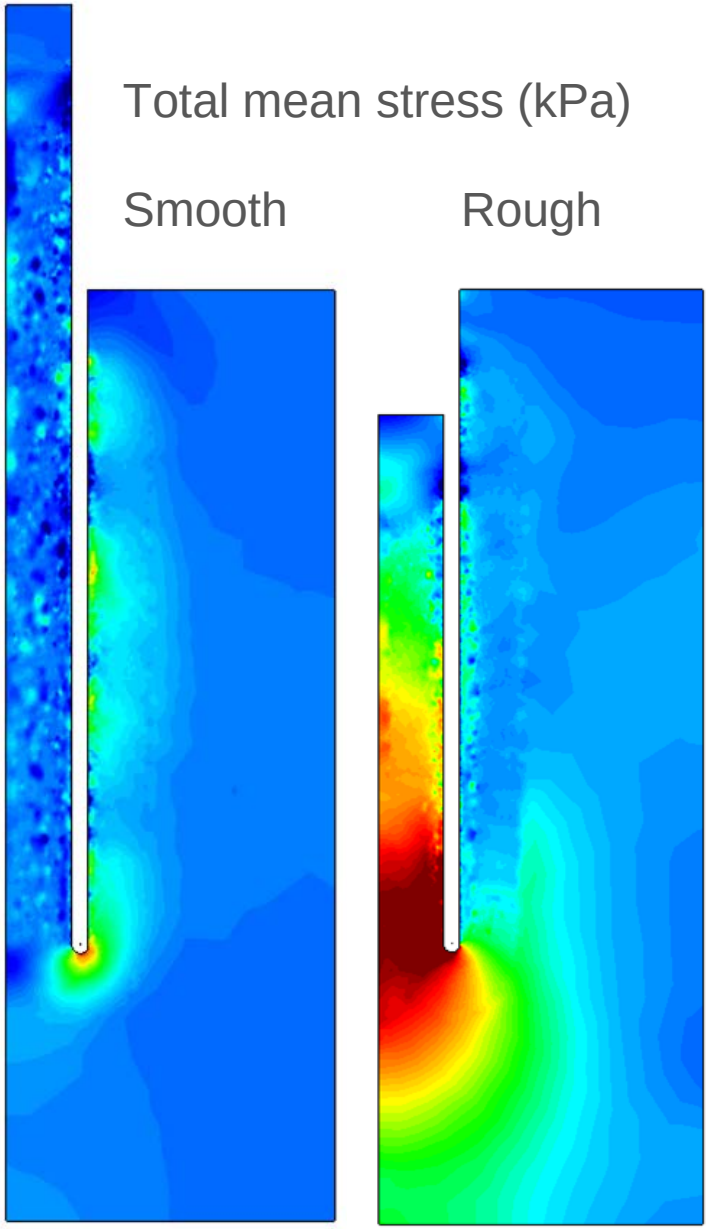

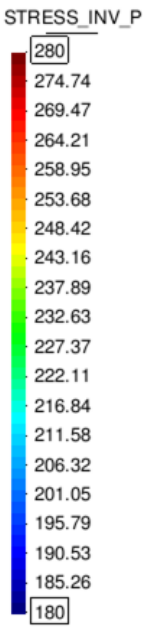

J2 (kPa)

Smooth

Rough

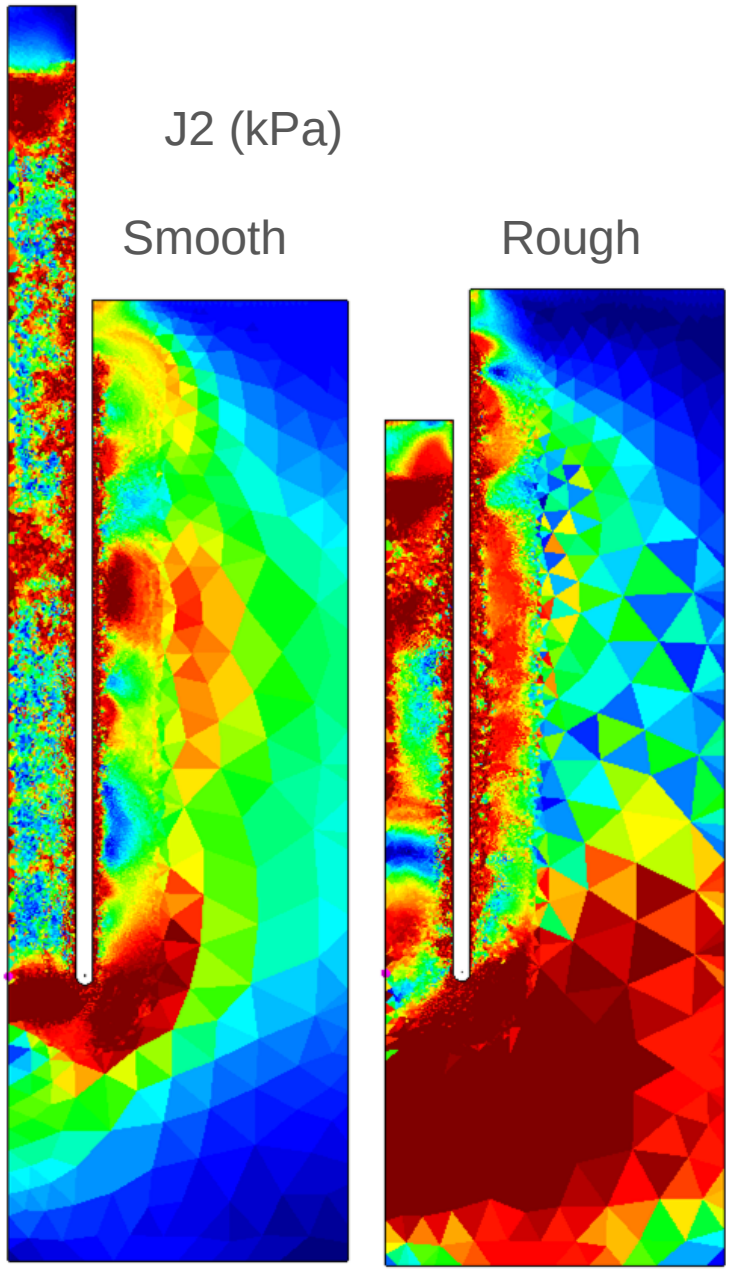

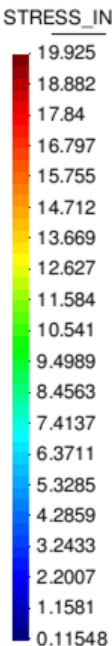

Influence D/t, Smooth interface

Increasing the ratio D/t decreases the amount of vertical elongation along the centreline.

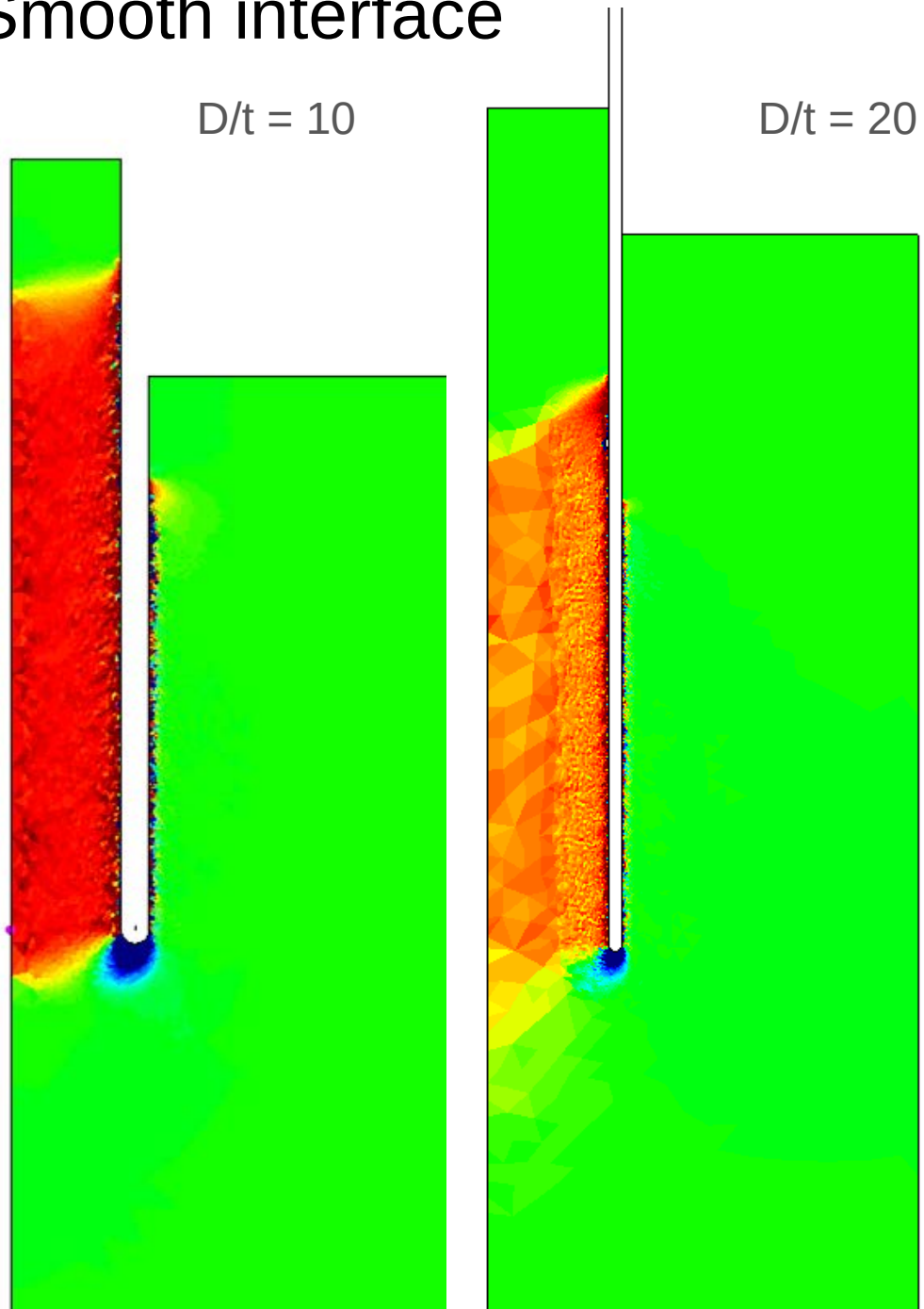

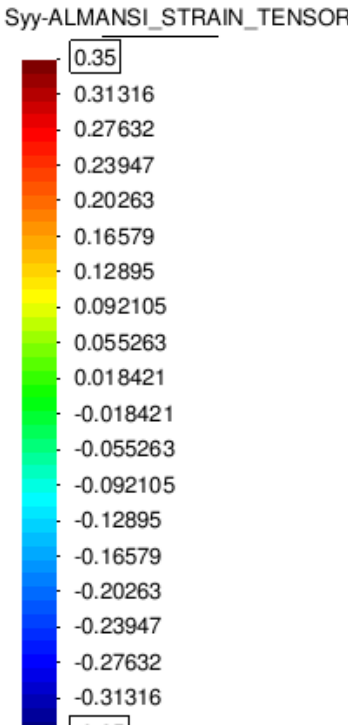

Influence D/t, Smooth interface

D/t = 10

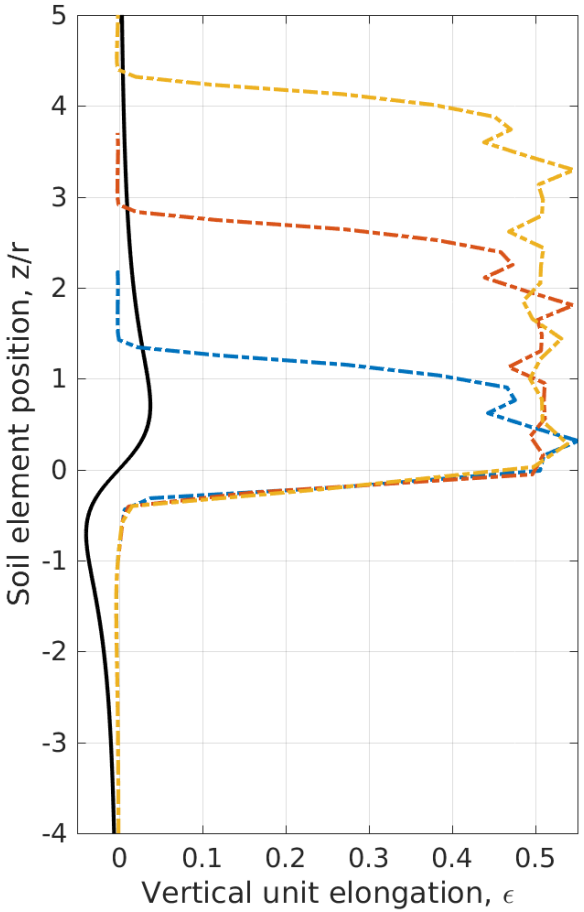

D/t = 20

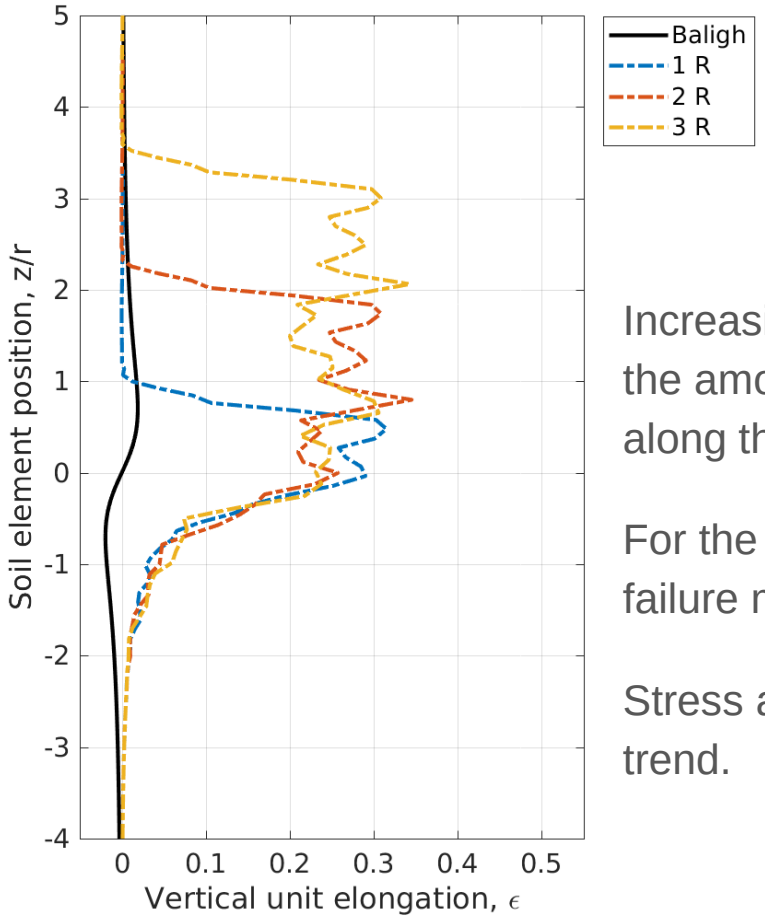

Increasing the ratio D/t decreases the amount of vertical elongation along the centreline.

For the case D/t=20 the same failure mechanism is found.

Stress and strains follow the same trend.

Hover et al (2013)

Small-scale physical modelling centreline strain path show a similar trend.
D/t = 14.5

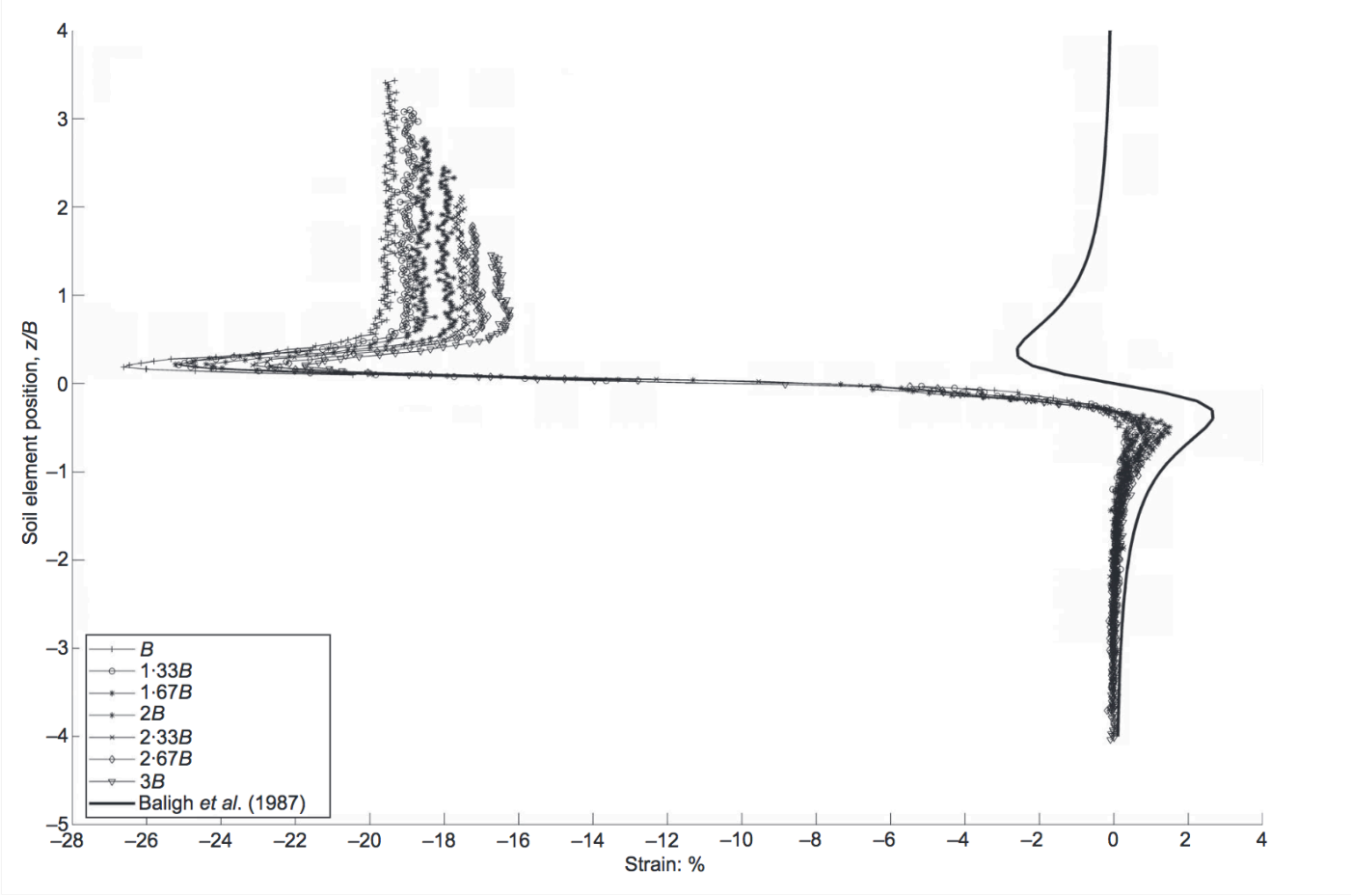

Influence of the shape of the cutting shoe

D/t = 10; Smooth interface; edge tapper angle 20º

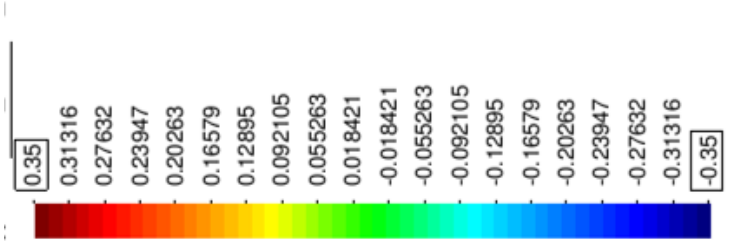

Components of the Almansi strain.

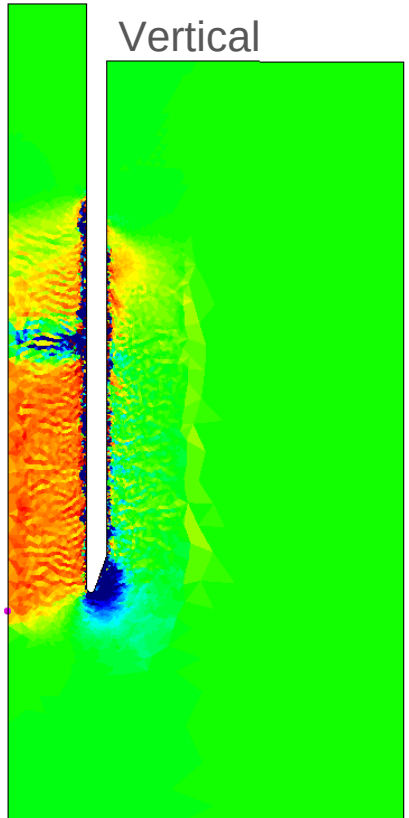

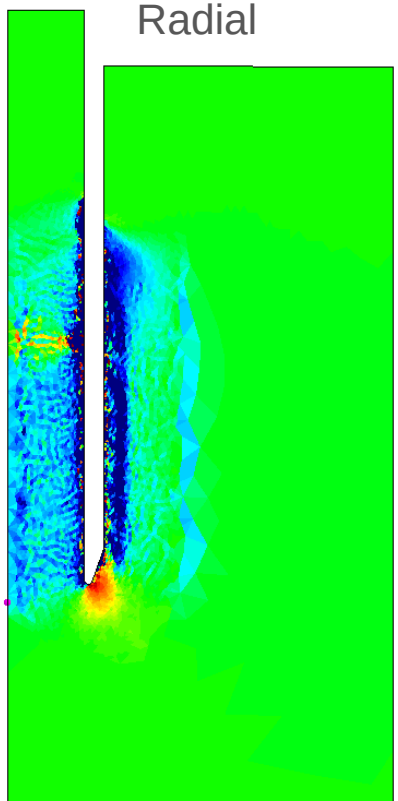

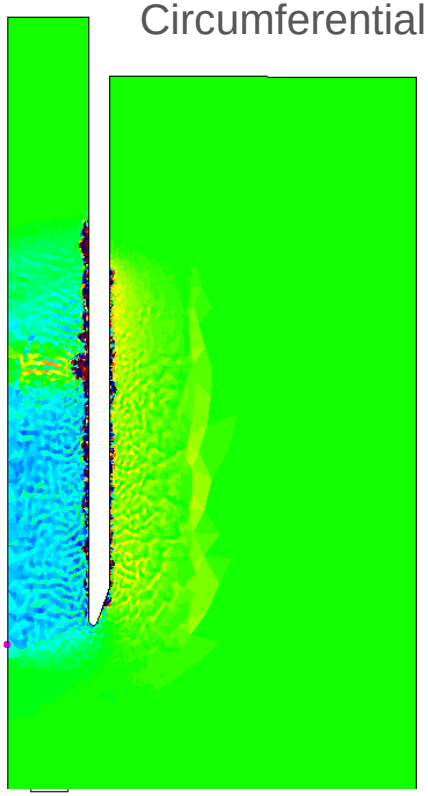

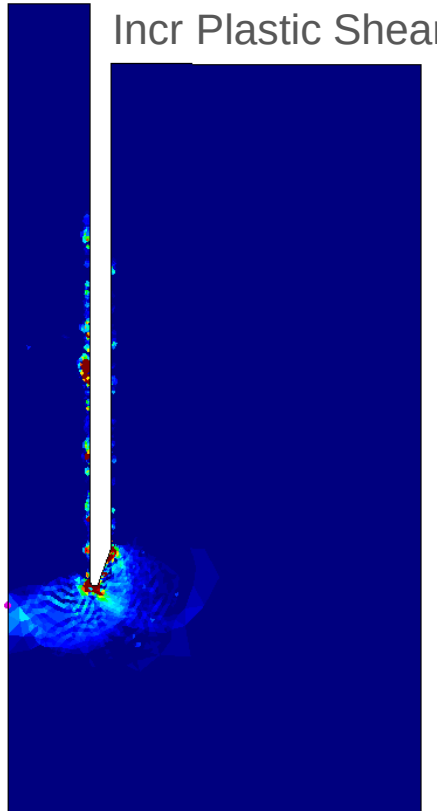

Influence of the shape of the cutting shoe

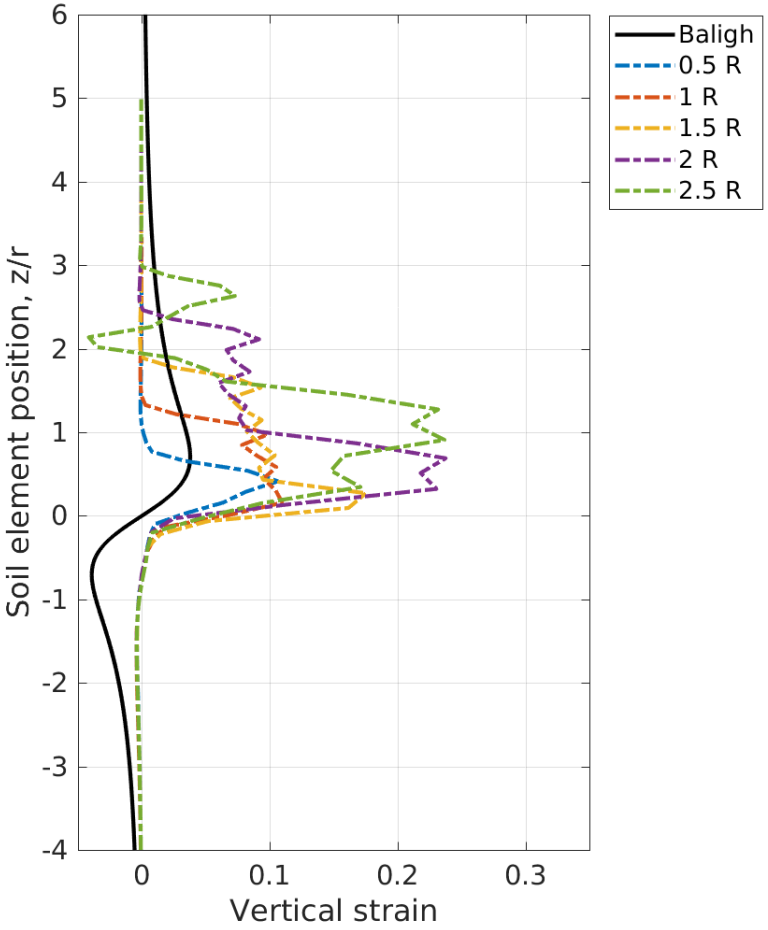

Smooth interface

The cutting shoe and the roughness of the contact has a large incidence on the strains inside and outside the sampler device.

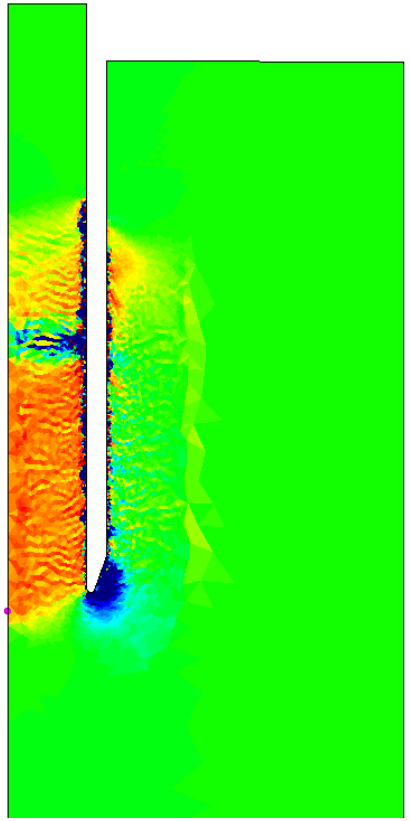

Piston

- Another way to reduce the deformation of the sample is the inclusion of a piston in the interior of the tube.

D/t = 20.0, Rough contact.

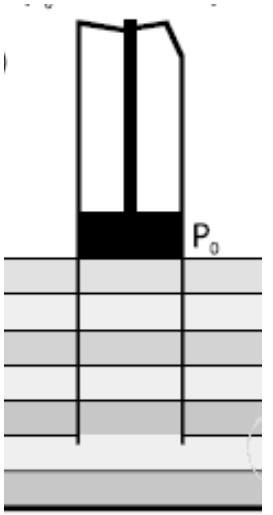

Skinner & McCabe (2003)

Components of the Almansi strain.

Vertical

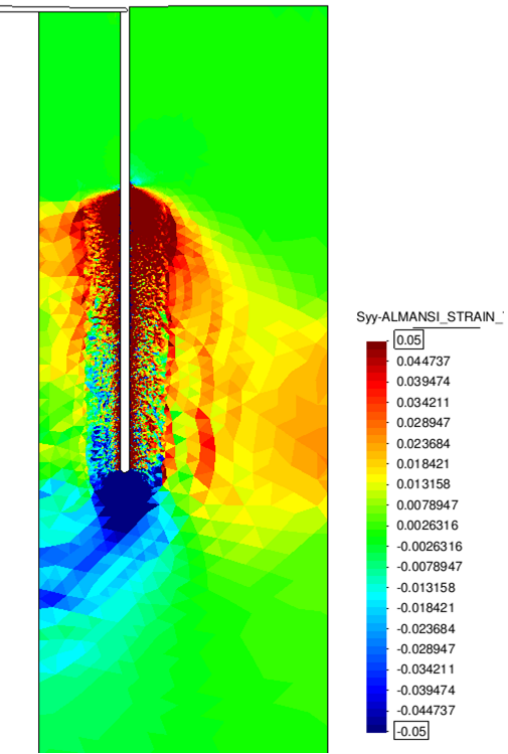

Radial

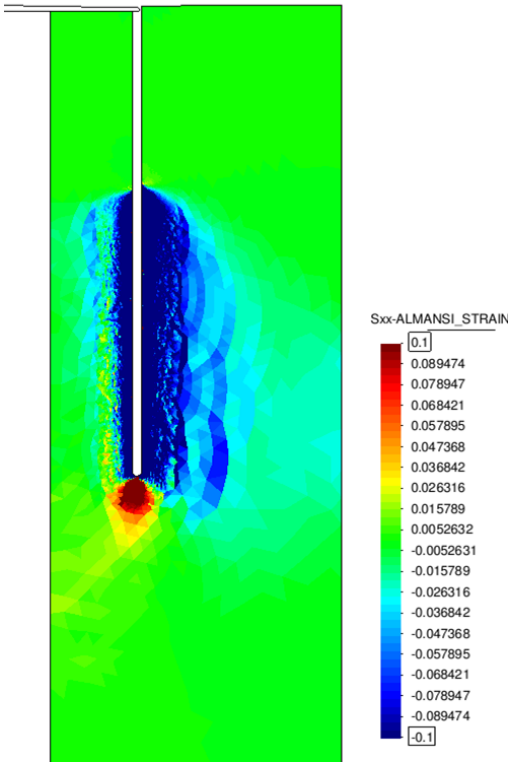

Circumferential

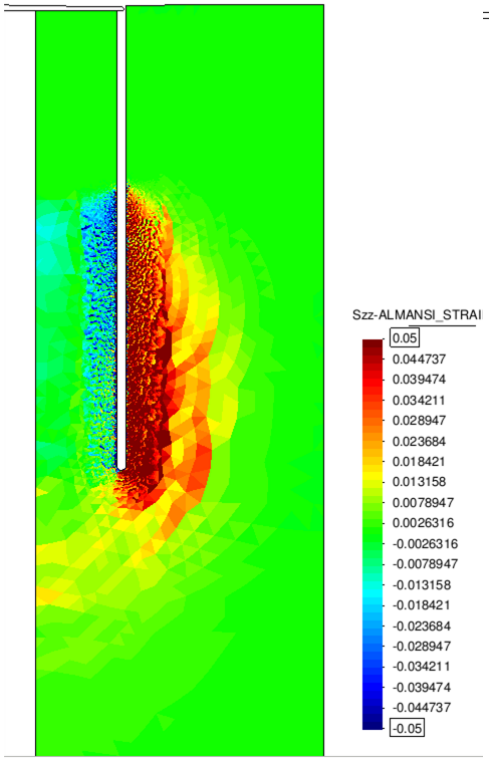

Shear

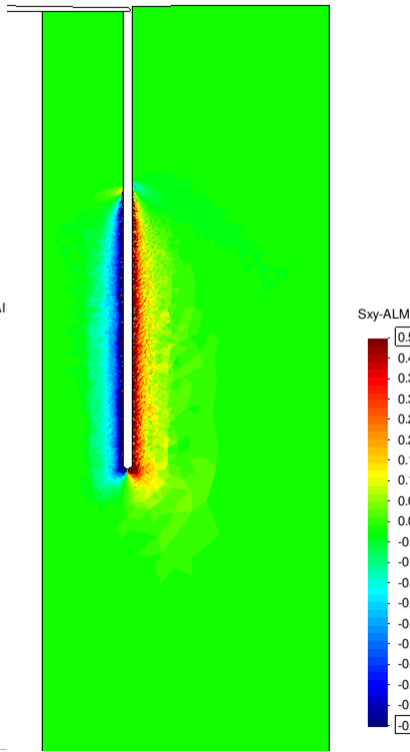

Piston

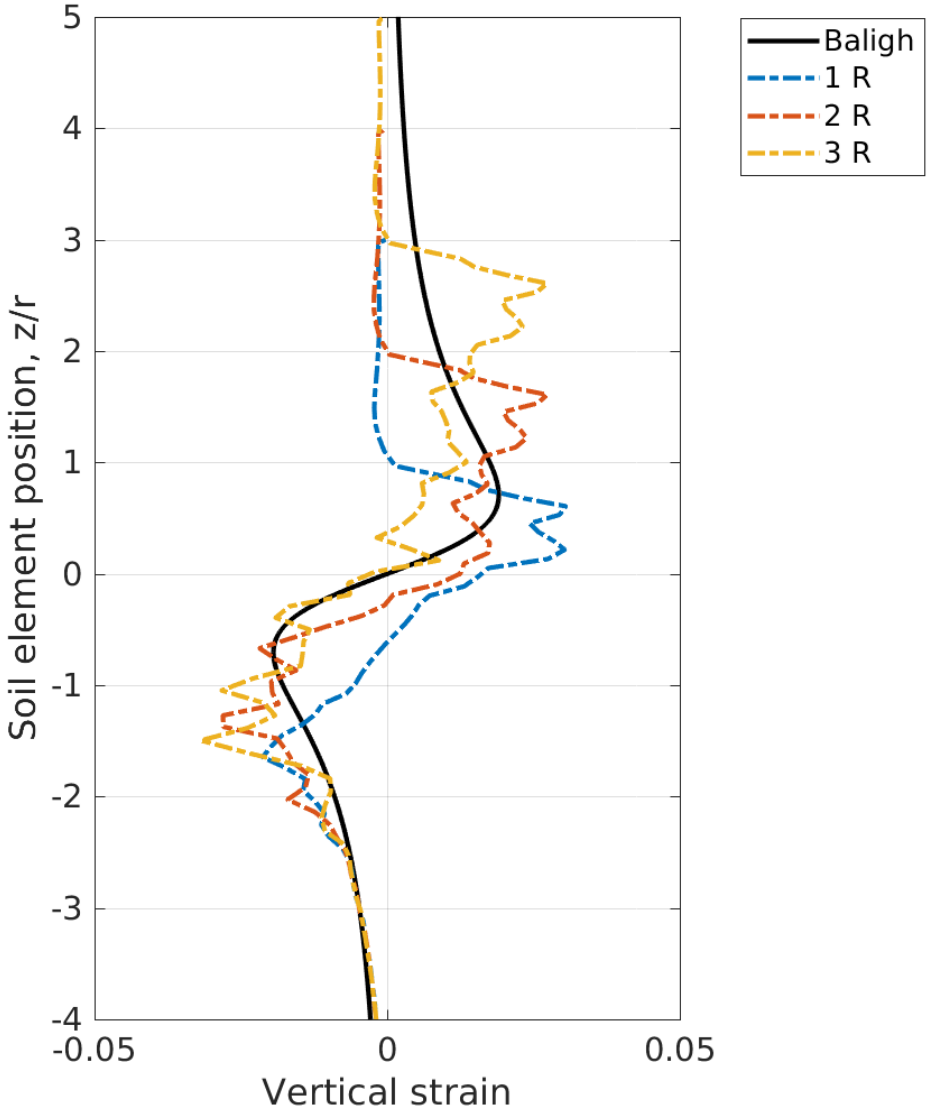

The inclusion of a piston decreases severely the vertical strains along the centreline of the sample.

In fact, the maximum magnitude is similar to that predicted by Baligh et al (1987) by the Strain Path Method.

Conclusions

- A numerical framework for the analysis of saturated porous media undergoing finite strains, based on PFEM, has been presented.
- Several mixed formulations for the single-phase mechanical problem and coupled hydro-mechanical problem have been described.
    - The benefits of the use of mixed-stabilized formulations has been shown in a total stress analysis of a rigid footing in a Tresca soil and the most challenging hydro-mechanical simulation of the CPT in a MCC soil.
- Preliminary results of the simulation of the soil sampling process have been discussed.
- The developed scheme appears to be a promising tool for the simulation of penetration problems in geotechnics.

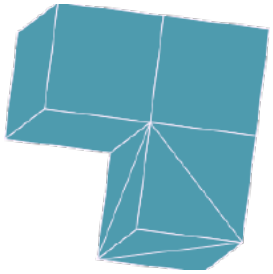

Kratos Multiphysics
https://github.com/KratosMultiphysics

Publications

- Monforte, L., Arroyo, M., Carbonell, J.M. & Gens, A. (2017) Numerical simulation of undrained insertion problems in geotechnical engineering with the Particle Finite Element Method (PFEM) *Computers and Geotechnics,* 82:144-156.
- Monforte, L., Carbonell, J.M. , Arroyo, M. & Gens, A. (2017) Performance of mixed formulations for the particle finite element method in soil mechanics problems. *Computational Particle Mechanics,* 4(3):269-284.

G-PFEM: a Particle Finite Element Method platform for geotechnical applications.

L. Monforte, M. Arroyo, J.M. Carbonell[1] & A. Gens
Universitat Politècnica de Catalunya, BarcelonaTech
[1]CIMNE, International Center for Numerical Methods in Engineering